This article is published on:

J. Geophys. Res., 108 (B9), 2454, doi:10.1029/2002JB002348, 2003

Source parameters of the 11 June 1909, Lambesc (Provence, southeastern France) earthquake: a reappraisal based on macroseismic, seismological and geodetic observations

Emmanuel Baroux*, Nicola Alessandro Pino*, Gianluca Valensise*

** Istituto Nazionale di Geofisica e Vulcanologia, Sezione Roma 1, Roma, Italy*

Oona Scotti** and Marc E. Cushing**

*** Institut de Radioprotection et de Sureté Nucléaire, BERSSIN, Fontenay-aux-Roses, France*

Abstract

Destructive earthquakes are rare in France yet pose a sizable seismic hazard, especially when critical infrastructures are concerned. Only a few destructive events have occurred within the instrumental period, the most important being the 11 June 1909, Lambesc (Provence) earthquake. With a magnitude estimated at 6.2 [*Rothé*, 1942], the event was recorded by 30 observatories and produced intensity IX effects in the epicentral area, ~30 km north of Marseille. We collected 30 seismograms, leveling data and earthquake intensities to assess the magnitude and possibly the focal mechanism of this event. Following this multidisciplinary approach, we propose a source model where all relevant parameters are constrained by at least two of the input datasets. Our reappraisal of the seismological data yielded M_W 5.7-6.1 (6.0 preferred) and M_S 6.0, consistent with the magnitude from intensity data (M_e 5.8) and with constraints derived from modeling of coseismic elevation changes. Hence, we found the Lambesc earthquake to have been somewhat smaller than previously reported. Our datasets also constrain the geometry and kinematics of faulting, suggesting that the earthquake was generated by reverse-right lateral slip on a WNW-striking, steeply north-dipping fault beneath the western part of the Trévaresse fold. This result suggests that the fold, located in front of the Lubéron thrust, plays a significant role in the region's recent tectonic evolution. The sense of slip obtained for the 1909 rupture also agrees with the regional stress field obtained from earthquake focal mechanisms and microtectonic data as well as recent GPS data.

1. Introduction

France is characterized by only moderate seismic activity and destructive earthquakes are fortunately rare. One seismic region of France is in Provence (southeastern France) where the strongest event of recent French history struck. On 11 June 1909, a strong earthquake hit a region located about 30 km northeast of Marseille, killing 46 people and causing extensive damage. The event immediately became the object of intense investigations, beginning with the pioneering works of *Angot* [1909a, 1909b, 1910], *Lemoine* [1910], *Lallemand* [1911] and *Spiess* [1926].

Owing to its size and the rapid diffusion of early seismographs that characterized that period, the event was recorded by several European observatories, so that seismologists could later derive objective estimates of its severity. Surface wave magnitudes based on one or a few recordings were given by *Rothé* [1942] (6.2), *Karnik* [1969] (6.2), *Massinon* [1979] (6.2), *Cara et al.* [1987] (6.3). Based on the analysis of the earthquake intensity distribution, *Levret et al.* [1994] proposed an equivalent magnitude of 5.5, an estimate then incorporated into the catalogue of French earthquakes compiled by *Levret et al.* [1996]. This relatively large discrepancy between instrumental and intensity-based magnitudes may be due to inherent uncertainties in the analysis of turn-of-the-century seismograms, written by instruments whose actual response in terms of magnification and damping factor is largely unknown. Alternatively, it could be explained by the sparseness of intensity observations or by the lack of a suitable calibration with the intensities of more recent French earthquakes.

In contrast, very little was written or hypothesized concerning the source mechanism and the tectonic framework of this event, although consensus exists on the orientation of active tectonic stress in the region and the compressional nature of faulting [*Baroux*, 2000; *Baroux et al.*, 2001a]. Recent analyses interpreted the 1909 event in the framework of purely

geological and tectonic evidence [e.g., *Carbon*, 1996], and even a very recent reappraisal by *Lacassin et al.* [2001] focused on only geomorphic and macroseismic evidence.

This paper aims to bridge the gap between the instrumental, macroseismic and field expression of the 1909 source by performing a joint and critical analysis of all available information. For a country with sparse seismicity like France, the 1909 earthquake represents a benchmark against which all ground motion estimates and design spectra for major facilities and ordinary buildings must be tested. For this reason, assessing the actual magnitude of the 1909 earthquake, estimating its rupture length and the extent of faulting at depth, understanding its tectonic and large-scale geodynamic context are all crucial steps toward a more accurate prediction of the ground motion associated with similar future events.

The intensity reports of the 1909 event are not re-investigated here as they are considered a reliable and homogeneous dataset. Instead our primary effort was to collect and re-analyze with standard seismological techniques all available instrumental observations, and particularly all historical seismograms that could be retrieved. We then compared the vertical displacement due to a model fault derived from intensity and instrumental data with nearly-coseismic elevation changes recorded in and around the epicentral region [*Lallemand*, 1911; *Romieu*, 1994]. Given the age and limited size of the earthquake rupture, none of these datasets constrains the desired source parameters when taken individually, but they all contribute to a joint interpretation. For this reason, we enforced a set of seismologically and tectonically coherent constraints and strived to find the best compromise among all available observations.

2. Geodynamic setting

The geodynamic history of western Provence, the region struck by the Lambesc earthquake, is relatively complex. Several phases of extension and compression occurred here during the past 50 million years. The general present-day framework is dominated by a set of E-W, south-verging folds resulting from the Pyreneo-Provençal orogenic phase (Eocene, about 50-40 Ma). The largest fold is the Lubéron, a 40 km-long massif located at the northern boundary of Provence (Figures 1, 2) rising from a "décollement" level at 5 to 6 km depth. Many other similarly trending folds occur between the Lubéron and the Mediterranean Sea such as Alpilles, Ste Victoire, La Fare Chainon, Costes and Trévaresse; the last two folds are closest to the epicentral region of the 1909 earthquake. Due to the absence of reported surface ruptures, so far the assignment of the event to one or another tectonic structure has been solely based on the damage pattern. Earlier studies did not determine an epicenter due to the large size of the highest degree isoseismal [*Carbon*, 1996], but recent studies point to the Trévaresse fold [*Baroux et al.,* 2001b; *Lacassin et al.*, 2001; *Chardon et al*., 2003].

Folding of this region is normally assumed to have taken place in a context of "thin-skin" deformation, but the existence of ramps affecting deeper crustal levels cannot be positively ruled out. The 3-D geometry of active thrust belts is especially important for anticipating the location and magnitude of impending earthquakes. Unfortunately, no seismic lines are available to illustrate the deep structure of these folds, so the presence and depth of their "décollement" level are still debated. A geological section drawn by *Champion et al.* [2000] across the Trévaresse fold proposes two possibilities: a 6 km-deep level corresponding to the prolonged Lubéron "décollement", or a shallower one at about 3 km depth.

By inverting focal mechanisms of mainly small earthquakes, *Baroux et al.* [2001a] computed the present-day regional stress-field of southeastern France. Although the region is globally dominated by compression, the authors identified quite distinct tectonic domains. On the one hand the western part of Provence (including the Lubéron, the E-W fold region north of Marseille and the Durance Valley) is characterized by a compression oriented N-S to NW-

SE, due to the rotating Italian peninsula and the Africa-Eurasia convergence. On the other hand, the Digne overthrust, located in the northeastern corner of the region, exhibits NE-SW compression and seems somehow controlled by the extensional regime that is deforming the Western Alps (Figure 1). Recent GPS results [*Nocquet*, 2002] confirm these orientations in southeastern France and the western Alps as well as the extreme variability of compressional trends within a relatively small region.

Finally, only few important events occurred during the past 500 years, about one per century. The magnitude of the largest earthquake recorded in the region in the modern instrumental era (since 1970) does not exceed M 4.5. For these reasons the 1909 Lambesc earthquake, the largest event to have occurred on-shore in southeastern France, provides a unique opportunity to explore present-day deformation and the potential for earthquakes in this region.

3. Damage distribution and analysis of intensity data

3.1. The intensity data

The macroseismic intensity data or earthquake felt reports comprise the first dataset we used to constrain the essential source parameters of the 1909 Lambesc earthquake. We considered all the intensities IV-V and higher (202 observations; Table 1) given by the SisFrance catalogue [*SisFrance*, 2000], a large nationwide compilation that rates about 85,000 felt reports for French earthquakes according to the MSK scale [*Medvedev et al.*, 1967]. However, following *Levret et al.* [1996], and as pointed out in the SISFRANCE database, we treated the intensities recorded at Vieux-Rognes (IX) and Vernegues (VIII-IX) as site amplification effects and considered them cautiosly in subsequent analyses.

Figure 2 shows the spatial distribution of all available data. All the isoseismals exhibit a distinct E-W elongation. Within this general trend, lower-degree isoseismals exhibit a

further level of asymmetry: the intensity VI isoseismal drawn by Levret et al. [1996], for example, extends for 23 km and over 40 km, respectively, to the east and west of the macroseismic epicenter. The intensity V exhibits a similar pattern, but its asymmetry is difficult to quantify given the sparseness of datapoints and lack of reports from the inner parts of the Alps.

3.2. The Boxer code

We used the intensity data to obtain a first estimate of the earthquake parameters using *Boxer* [*Gasperini et al.*, 1999], a Fortran program designed to assess the location, physical dimensions and orientation of the source of large historical earthquakes. Although the program was originally developed for and calibrated on Italian earthquakes, we recall that from a geodynamic, geological and seismological point of view southeastern France is more similar to northern Italy than to the rest of France itself. Potential over- or under-estimations may also arise from the awareness that French intensities are assessed according to the MSK intensity scale whereas the Italian catalogue [*Boschi et al.*, 2000] uses the MCS scale [*Sieberg et al.*, 1932]. An extensive comparison among over 50 of the most commonly used intensity scales drawn by *Ferrari and Guidoboni* [2000], however, shows that the definitions of the MCS and MSK scales overlap almost exactly.

First the earthquake epicenter is found through an averaging technique described by *Gasperini and Ferrari* [1995, 1997]. The spatial distribution of intensities is then used to infer the earthquake seismic moment M_o and the corresponding moment magnitude M_w. The source size is assessed using the empirical relationships M-rupture length and M-rupture width derived by *Wells and Coppersmith* [1994]. Given the variety of source mechanisms encountered in the investigation of Italian earthquakes, *Boxer* consistently uses empirical relationships derived for the "All" category of *Wells and Coppersmith* [1994], that is, a

category that mixes together all available data regardless of the fault kinematics and tectonic regime.

The definition of the source orientation is based on the assumption that for earthquakes having $M_W \geq 5.5$ the shape of the highest degree isoseismals is controlled by the fault's physical elongation along strike. Clearly, the orientation can only be resolved for sources that are longer than the average spacing between intensity datapoints. The source orientation is then computed as the circular mean of the highest degree intensity datapoints, provided that their spatial and azimuthal distribution is good enough to grant reliable results. This condition is checked automatically by the program through a series of statistical tests.

Due to the known trade-offs between earthquake depth and magnitude, currently *Boxer* does not determine the source depth. The Italian earthquakes that were used to calibrate *Boxer* all fall in the depth range 5-15 km, hence the magnitudes it determines are reasonably accurate only for earthquakes that fall within this range. Further details on *Boxer* and on its algorithm are given in *Gasperini and Ferrari* [1995, 1997] and *Gasperini et al.* [1999].

3.3. Results and interpretations

The experience gained using *Boxer* with Italian earthquakes shows that for earthquakes of the past 30 years, for which the instrumental estimates of magnitude/seismic moment are considered reliable, the scatter between measured and intensity-derived magnitude is always smaller than 0.3 units, and often on the order of 0.1 [*Gasperini et al.*, 1999; *Valensise and Pantosti*, 2001]. Our assessment of the magnitude of the 1909 earthquake will compare with a previous estimate of 5.5 obtained by *Levret et al.* [1994] based on the average radii of the isoseismals for intensity III and higher, and with a recent estimate of 6.0 obtained by *Griot-Pommera and Scotti* [2001], also based on intensity data exclusively.

We computed two solutions for the Lambesc earthquake, respectively considering (#1) the entire intensity dataset for I ≥ IV-V, and (#2) a dataset reduced after removing two outliers that probably reflect strong site amplification effects (see discussion above and Table 1). The resulting spatial (epicenter, source length, source width), geometric (strike) and energetic (equivalent magnitude M_e) parameters are summarized in Figure 2. The epicentral determination rests on the 6/4 (respectively for solution #1/#2) highest intensities data (VIII and up); similarly, the source orientation is based on the 16/14 highest intensities (VII and up). Lower intensities, that normally carry information on propagation rather than source characteristics, are hence not used in this step.

Solution #1 (all data, shown with dotted lines in Figure 2) carries a large uncertainty in the determination of source orientation. It sets the epicenter at the western end of the Trévaresse fold, but the source orientation is more than 20° off the trend of this structure and in fact is more similar to the trend of the Costes fold, located north and west of Lambesc. Solution #2 (solid lines in Figure 2) sets the epicenter at 43.635N latitude, 5.370E longitude, just on top of the Trévaresse fold, and the source orientation (N092±16°) is almost identical to that of the anticline. This second solution confirms a previous estimation by *Baroux et al.* [2001b], is in agreement with the study of *Lacassin et al.* [2001], and is not affected by large site amplifications that are an obvious source of inaccuracy.

The algorithm implemented in *Boxer* to compute the equivalent moment magnitude considers the six largest degree isoseismals (from intensity VIII to IV) to obtain an equivalent magnitude M_e of 5.8. The formal uncertainty supplied by *Boxer* for this estimate is less than 0.1 magnitude units, but the real scatter is probably on the order of ± 0.1-0.2. Finally, *Boxer* uses *Wells and Coppersmith*'s [1994] empirical relationships to derive a source length and width of 9 km and 7 km, respectively, yielding a fault area of 63 km^2.

4. The seismographic record

4.1. The seismograms: retrieval and processing

The Lambesc earthquake was recorded at over 30 European stations. In the early stages of this work we made an inquiry to all European observatories within 2,000 km of Lambesc to know whether the earthquake had been recorded at the given station and, if so, whether the original seismograms still exist. Thanks to the generosity of a number of seismologists and technicians (individually listed at the end of this paper), we collected 30 seismograms from 14 observatories (Table 2). For some stations, such as those located in UK or central Italy, the signal was too small to be retrieved. In contrast, the Vicentini seismograph of the Ebre station (EBR) was blocked by the resonance caused by the lack of a damping device. The stations that returned the best seismograms are all located in the distance range 600 to 1,200 km.

Before processing the seismograms in preparation for modern seismological analyses, we recovered all basic characteristics of the instruments at the time of the earthquake (mass, period, damping constant and amplitude - see Table 2 and Figure 3). Most of these parameters were available and were supplied with the seismograms or found in the literature (such as in the case of Ebre - EBR, Goettingen - GTT, Hamburg - HAM, Paris - PAR, Strasbourg - STR and Vienna - VIE). For the remainders, such as for De Bilt - DBN, the constants we used were calculated almost thirty years later on the same seismometer, but we do not expect this delay to affect significantly our results. For Uppsala - UPP, we found two different but very similar series of parameters; we tested specifically the impact of using one or the other and found out that an arbitrary choice does not influence the results appreciably. The Wiechert instrument was the most commonly used seismometer at the time of the Lambesc earthquake, but we also collected seismograms written by Vicentini (Ebre - EBR) and Bosch (De Bilt - DBN) instruments.

Out of 30 seismograms, we found 20 suitable for digitization(Table 2; Figures 4, 5) and, except for Ebre (EBR), for computing the surface wave Magnitude Ms. Regarding the Ebre seismograms, the recording terminated with the arrival of the S waves, and for this reason they were not used to compute the Ms. In addition, we computed the Ms on seismograms written by the Wiechert-17 tons of Goettingen (GTT) and at the station of Munich (MNH), adding up to a total of 20 recordings suitable for computing the surface wave magnitude (Figure 6; Table 3). The seismograms that were finally used for the analysis were supplied by 11 observatories (Table 2; Figure 5). Unfortunately, some of them (VIE, PAR) were actually copies of the originals reproduced at an unknown scaling ratio. We have been able to overcome this problem for PAR thanks to a paper by *Angot* [1909a], who meticulously reported the characteristics of the Wiechert seismometers measured the day of the earthquake. His precise assessment of the paper velocity allows the reproduction ratio to be accurately determined, and hence the waveform amplitude to be correctly measured. In contrast, no such clue was available for restoring the original amplitudes for VIE. For this station we made an inference based on the notion that all seismograms recorded by Wiechert instruments similar to that operating in Vienna have nearly the same paper velocity. From our database of 1909 seismograms we inferred a maximum (0.257 mm/s) and minimum (0.158 mm/s) value for paper velocity, which allowed us to derive an amplitude range and hence a magnitude range (see #19, 20 in Table 3). Despite the uncertainties on signal amplitude, we computed synthetics for these seismograms because the ratio of the various components is independent of the scale.

The digitization was made in collaboration with the staff of the SISMOS Project of INGV in Rome. The seismograms were scanned and digitized through a methodology developed by SISMOS [*Bono et al.*; 2002; *SISMOS Project web site*, 2002]. The applied sampling frequency is large enough not to influence the recorded signals at the frequency of interest of our analysis. The displacement speed of the paper on the seismometer is checked

minute by minute. The effect of the arm finite length was corrected using an algorithm also developed by SISMOS. Overall, the uncertainties involved in the digitization process do not seem to bear significant influence on the amplitude and frequency of the waveforms.

4.2. The surface wave Magnitude Ms

4.2.1. The mainshock of 11 June 1909

The first published magnitude for the 1909 earthquake is M_S 6.2 given by *Rothé* [1942]. Later on *Karnik* [1969] used the Prague formula to estimate M_S 6.2 using 12 data from observatory bulletins. More recently, *Massinon* [1979] and *Cara et al.* [1987] also proposed M_S estimates of 6.2 and 6.3, respectively. Although there appears to be a good consistency among different investigators, it should be pointed out that in all of these cases the analysis was either based on seismograms from one or a few stations (e.g. STR and PAR), or on unverified amplitude readings routinely reported in bulletins.

Thanks to the data gathering effort described above, we have been able to obtain an M_S estimate for 20 seismograms from 10 stations (Tables 2, 3; Figures 5, 6). The M_S was computed using the Prague Formula

$$M_s = \log\left(\frac{A}{T}\right)_{\max} + 1.66\log\Delta + 3.3$$

where A is the amplitude, T its period and Δ the epicentral distance (in degrees), and the Karnik method [*Karnik*, 1969]. According to this method i) for each station the instrumental response at the wave-period corresponding to $(A/T)_{max}$ is taken into account, and ii) statistical corrections are applied, as suggested by Karnik based on all estimations for a given station. Table 3 illustrates the results of our computations and supplies details of the calculation for each individual station. The average of 20 estimates gives M_S 6.0.

4.2.2. The largest aftershock

Some of the early investigators [e.g.: *Angot*, 1909a, 1909b, 1910; *Lemoine*, 1910] and a few bulletins report a strong tremor that occurred about 31 minutes after the Lambesc mainshock. Although this is normally identified as the largest aftershock of the 1909 sequence, no macroseismic investigation was carried out for this event because of its early occurrence after the mainshock. *Lacassin et al.* [2001] hypothesized that this event was comparable in size to the mainshock and that it ruptured the eastern portion of the Trévaresse thrust.

We were able to study this aftershock thanks to the availability of the entire recording of the station De Bilt (Wiechert seismometer) and of some observatory bulletins (DBN, HAM and LEI). The De Bilt seismogram shows that the maximum amplitude of the aftershock is about 40 times smaller than that of the mainshock. The average surface wave magnitude computed based on two seismograms plus three bulletin readings and using *Karnik*'s [1969] corrections is M_S 4.4 (see Table 4). All the remaining 16 aftershocks reported by the SisFrance catalogue [*SisFrance*, 2000] are smaller or at the most comparable in size with the Lambesc aftershock analyzed here. This confirms that aftershock activity was minor and hence negligible in terms of fault length and ground displacement with respect to the mainshock.

4.3. Moment magnitude M_w and waveform analysis

The estimation of moment magnitudes requires a structural model and a focal mechanism. The propagation of seismic waves in the crust and upper mantle affects significantly the ground motion recorded at regional distances. Isolating the source contribution in the waveforms thus requires the determination of a reliable model of the velocity structure. As proposed by previous authors (e.g. *Pino et al.,* [2000]), one way to

estimate the velocity model is through the analysis and modeling of well-recorded events of known source mechanism and source-to-station paths similar to those characterizing the earthquake of interest.

4.3.1. The structural model

Although these data are very scarce in such a low seismicity region, one suitable recording for the 13 April 1992, Roermond, the Netherlands, earthquake (M_W 5.4: Harvard CMT) does exist. The seismic path of this recording from Roermond to the broad-band station of Saint Sauveur (SSB, central France, Geoscope network) is reasonably similar to the path from the epicenter of the 1909 earthquake to the De Bilt station (Figure 5). Starting from the global structural model IASP91 [*Kennet and Engdahl*, 1991], we developed by trial-and-error a 1-D model for the crust and upper mantle structure representative of the SSB-to-Roermond path. This model provides a much better fit to the data, both in terms of arrival times and amplitudes. During the entire modeling procedure for structure investigation, as well as for the following source analysis, we used a code based on the F-K integration method (frequency-wavenumber domain). We focused on modeling absolute and relative amplitudes of major arrivals; in this study we are not interested in the structure itself and hence we will not discuss the models we used.

Figure 7 shows the comparison between data and synthetics obtained for the 1992 earthquake using our preferred model. The synthetics were computed based on the Harvard CMT focal mechanism. To test the limitations of the model for our purposes we show the 3-component ground displacement broadband waveforms along with the simulated signals for the Bosch and Wiechert instruments operating at De Bilt in 1909. The fit to the broadband displacement data is very good, ensuring that all major structural features are well accounted for by our model. The synthetics have been scaled to the Harvard CMT seismic moment of

1.32×10^{17} Nm. The maximum amplitude difference between the recorded and computed waveforms is about 30%. This uncertainty results in a 0.1 uncertainty in the M_W estimates. Concerning the simulation of the De Bilt instruments, the Bosch synthetic waveforms are in very good agreement with the data, while the Wiechert synthetics do not reproduce the relatively high amplitude phases, probably due to a very different instrumental response (Table 2). Nevertheless, the maximum amplitude phase is correctly reproduced, thus yielding the correct seismic moment and moment magnitude.

As mentioned earlier, no usable modern data are available for the other Lambesc earthquake source-to-station paths. After several tests, however, we found that the model developed for DBN provides a satisfactory fit also for PAR, STR and HAM, and hence retained it for these stations. The fit of the GTT, EBR, LEI, POT, VIE and UPP waveforms, on the other hand, is rather poor. For this second group of stations we finally decided to use the global model IASP91. In principle, both the phase and the amplitude of surface waves are affected by the crustal and upper mantle structure at the analyzed periods. As discussed in the following sections, however, we expect the effects of this approximation to be negligible for the estimation of source parameters.

4.3.2. The source mechanism

At fixed azimuth, the focal mechanism strongly affects the partitioning of energy on the different components of the seismic motion. As a consequence, very large differences in the estimated seismic moment may result from different hypotheses on the source geometry. To test the variability of the waveforms for changes in strike, dip and rake of the rupture plane and set further constraints on the source mechanism, we compared synthetic seismograms computed for a number of different focal mechanisms with the waveforms recorded at GTT and DBN. For the 1909 earthquake waveforms we preferred to convolve the

synthetic seismograms for the relevant instrumental response rather than correct the data. These two stations are the most suitable for this test: for DBN we could rely on a calibrated structural model, whereas GTT is the only station for which we have all three components of ground motion, allowing for a better evaluation of the amplitude ratio between the different arrivals. For DBN we used the recordings of the Bosch seismograph, characterized by a longer natural period with respect to the Wiechert installed at the same location, and hence less affected by small-scale structural heterogeneities. This station is particularly important because the N and E directions are naturally rotated along the radial and transversal directions with respect to the 1909 source. Although the Lambesc earthquake clearly occurred within the shallowest 10 km of the crust, the available seismograms do not allow a precise determination of source depth. For this reason we fixed the source depth at 6 km throughout the entire modeling procedure, as suggested also by geological evidence and by modeling of geodetic data.

Although several lines of evidence suggest that the 1909 Lambesc event was generated by slip on a roughly E-W striking plane with a thrust mechanism, as a first step we tested three fundamental faulting styles for the same 270°-striking fault. Figure 8 shows synthetic waveforms for 270°-striking, pure normal and pure thrust faults, both dipping 45°, and for a 270°-striking, subvertical pure strike-slip fault. The thrust fault produced the most realistic waveforms, but it appears that a strike slip component is needed to obtain a more correct amplitude ratio between the different components. In particular for GTT the seismograms indicate different relative amplitudes between the various arrivals recorded on the north component, and require that the amplitude of the vertical component be reduced with respect to the east component.

We then refined our analysis by testing several mechanisms obtained by varying progressively the parameters of our best fitting preliminary model fault (E-W-striking, 45°-dipping pure thrust). We computed synthetic waveforms for 27 different mechanisms

obtained from all possible combinations of three strike (250˚, 270˚, 290˚), three dip (30˚, 45˚, 60˚) and three rake (45˚, 90˚, 135˚) angles. Figures 9 and 10 show the fit to the data. As for GTT, better fits are obtained for mechanisms displaying a dextral component of slip (focal mechanisms identified by multiples of 3), which consistently return more appropriate amplitude ratios between the N and the E components and between the different arrivals on the N component. Also, lower amplitude is predicted by this type of mechanisms on the vertical component, as observed in the data. All in all, we believe that the best compromise is represented by the double couple #27 (strike 290˚, dip 60˚, rake 135˚), that produces a satisfactory fit to the data for both stations considered in this test. Unfortunately, the uncertainties accumulated in the process of scanning, digitizing and correcting the waveforms, evaluating the theoretical instrumental response and estimating the characteristics of the structural model do not allow a firmer assessment of the focal mechanism. However, the result of this analysis is the determination of a roughly EW - most likely N110° - oriented thrust fault with a little dextral component as the most likely source mechanism of the 1909 Lambesc earthquake.

4.3.3. The seismic moment and the moment magnitude M_W

We used the previously determined structural models and focal mechanism to compute synthetic seismograms for all usable recordings. By matching the amplitude of the main arrivals we evaluated the seismic moment for each waveform (Table 3, Figures C). Except for EBR, the resulting values are in the range 0.7-25.0 x 10^{17} Nm, corresponding to a moment magnitude M_W in the range 5.16 to 6.20. The extreme values often result from stations with relatively short period instruments: the vertical component at GTT and both horizontal components of DBN were recorded by instruments having natural period of about

5 s. At such short periods the signal is much more sensitive to the local crustal structure below the station, which is not taken in to account in our structural model.

The seismograms of the EBR station require specific comments. Among all available stations, the Ebro instrument had the shortest natural period and was completely undamped, the only effective damping resulting from the internal and stylus/paper frictions, a condition that may easily lead to major errors. Besides, only the portion of the signal relative to the P wave-train was suitable for digitization; the determination of seismic moment hence relies exclusively on modeling of P wave arrivals, which are highly affected by small-scale structural heterogeneities and by even small variations of the focal mechanism. For these reasons we will disregard the seismic moment computed at this station.

The results obtained for the long period instruments fall in the range 0.7-15 x 10^{17} Nm (M_W 5.16-6.05), with an average of 4.69 x 10^{17} Nm (M_W 5.71) (Table 3). In spite of this variability, the procedure shows some consistency in the magnitude estimation while highlighting a distinct dependency on station azimuth for both M_W and M_S. In fact, a clear pattern of decreasing magnitude is evident as azimuth increases from north (Figure 12). Due to the fact that both M_W and M_S are computed starting from the maximum amplitude, it is not surprising that local oscillations are quite similar, though M_W appears to decrease faster than M_S for an increasing azimuth; they display a difference of about 0.2-0.4, M_W being consistently much smaller than M_S, with the only exception of the Bosch instrument at DBN. In computing synthetic seismograms we assumed a fixed source duration of 5 s, which is commonly observed for events in the range 5.5<M<6.0. Actually, if the rupture propagated westward the observed amplitudes should decrease as azimuth increases, with a minimum at 90º from north; smaller moments would then result when synthetics with constant source duration are matched to the data. We then included the effect of source directivity by assuming a fracture propagating to the west. Figure 12 shows M_W values (dotted line)

corrected for the effect of directivity. The new values differ very little from the old ones while, if this effect were the only one responsible for the observed trend, an approximately constant M_W would have resulted.

We conclude that the causes for the observed variability in M_W could include:

i) the effect of an inaccurate focal mechanism in the computation of synthetics;

ii) the compounded uncertainties in the theoretical instrumental response (mainly magnification and damping);

iii) poor knowledge of the regional and local structure of the crust and upper mantle.

We have no means of testing the correctness of the instrumental response, which can only be responsible for local variations of M_W rather than for a continuous trend. At regional distances, for a given source mechanism the surface waves at the period corresponding to the maximum amplitudes (essentially 8-10 s) can be seriously affected by the structure of the crust and upper mantle. As a matter of fact, the paths considered here cross quite diverse tectonic structures; in particular, we encounter a thicker and more attenuating crust as azimuth increases, for instance as the ray-path crosses the Rhine graben and the Alps. We recall here that only the structural model for DBN could be tested; this model was also used for computing synthetics for PAR, STR and HAM, but provided very poor fit for the other stations, for which we used IASP91. After testing several other models characterized by a very different velocity structure and thickness, and also different source depths, we obtained a set of M_W estimates fluctuating by 0.2-0.3 units. Given the different hypothesis, we can conclude that the moment magnitude estimate for this event is therefore between M_W 5.7 (average of all long period data) and M_W 6.0 (DBN value, obtained by using a calibrated structural model, +0.1 uncertainty). The most reliable estimate being the latter because based on a long period instrument and a reliable structural model. This value is also consistent with the average M_S estimate.

In its turn, the observed azimuthal trend in M_S could be explained by:

i) wrong instrumental response (not verifiable);

ii) strong lateral variations in the crust and upper mantle structure;

iii) source directivity (only for the general trend, not for local anomalous values).

As mentioned in the previous section, we used station corrections for M_S and somehow they should take into account the local structure. The azimuthal variation of the resulting M_S can certainly be explained by the lateral heterogeneity of the structure, however we also checked for the possible presence of source directivity. Figure 13 shows a comparison of the S waves recorded ad GTT and DBN. These two stations have similar distance with respect to the epicenter of the Lambesc earthquake and lie in the same northeastern quadrant (azimuth 20° and 359°, respectively). Even though recorded by an instrument with a shorter natural period (Table 2), GTT displays longer pulse duration with respect to DBN. This is compatible with a westward propagation of the rupture which would produce a difference in the apparent source duration of the S pulses at the two stations up to about 1.5 s. We also analyzed the P wave-train observed at EBR, located in the southwestern quadrant (azimuth 235°). The source duration needed to obtain a satisfactory fit is 1-2 s, significantly shorter than the 5 s assumed earlier (Figure 14). Moreover, P waves are hardly detectable on all the seismograms recorded at stations located in the northeastern quadrant. Although we are aware that the evidence is weak we maintain that a westward propagation of the rupture is a reasonable hypothesis. Considering the preferred fault strike (110˚), this would also imply a considerable updip component. This finding would also be compatible with the slight E-W asymmetry seen in the isoseismals, a feature unmodeled by *Boxer* (Figure 2; see also Section 3).

4.4. Conclusions from seismographic analyses

The analysis of regional seismograms for source investigation is often a very difficult task. In our case, the lack of modern digital data to be used for calibrating the structural model and the very poor content of P and PL wave motion in the recovered historical seismograms did not allow a detailed analysis of the source characteristics. Nevertheless, we demonstrated that useful information can still be retrieved with modern techniques from a set of nearly century-old seismograms.

We first followed a forward modeling approach to test a number of different hypotheses and to set basic constraints for the source parameters. This step demonstrated that the 1909 Lambesc earthquake occurred on a thrust fault with a dextral component of slip. The similarity between the seismic moment resulting from the horizontal components of stations where both of them were available supports our preferred focal mechanism, which is also in agreement with the regional stress field obtained from the inversion of focal mechanisms [*Baroux et al.,* 2001a].

As for the seismic moment, we constrained it in a relatively narrow range that appears to agree with all available geophysical data. Using a different structural model would probably have changed the values resulting at each station, but the overall estimation would not have changed significantly.

Finally, as a working hypothesis we suggest a west-southwestward and updip propagation of the rupture, which would be consistent with the asymmetry of the macroseismic field.

5. The 1909 Lambesc earthquake source: a summary

Based on the multidisciplinary approach described so far, we can now propose a model for the source of the 11 June 1909 Lambesc earthquake. The model devised here will then be used as input for predicting coseismic strains to be compared with the elevation changes observed by *Lallemand* [1911].

The good macroseismic data made available by *SisFrance* [2000] constrain the epicentral area to coincide with the region overlying the Trévaresse thrust and fold. The Trévaresse (Figure 1) is globally composed of two segments: a western one oriented about N110° and an eastern one striking N090°, having a length of roughly 10 and 6 km, respectively. In addition to the evidence supplied by the earthquake itself, recent activity of this fold is suggested by recent morphotectonic investigations [*Lacassin et al.*, 2001; *Chardon et al.,* 2003].

The orientation of our model fault is constrained by intensity data (see §3.) and the focal mechanism tests made on the 3-components of the Goettingen station and the 2-components of the De Bilt station (§4.3.2.). The preferred focal mechanism (N110° or 290°) is consistent with the orientation of the western segment of the Trévaresse fold, but the source orientation suggested by macroseismic observations (92°±15) is not accurate enough to distinguish between the eastern and western segments. In contrast, the intensity-based epicenter again supports the hypothesis of earthquake rupture on the western Trévaresse; in particular, the eastern edge of the preferred macroseismic box (see Solution #2 in §3.3. and Figure 2) nearly coincides with the location of the ~20˚ bend between the two fold segments.

Our re-evaluated seismological magnitudes set an upper boundary of M_w 6.0, corresponding to a fault area of ~65 km^2. This result agrees with the 9 x 7 km estimates for fault length and width obtained from the intensity-derived magnitude (5.8) using the relationships proposed by *Wells and Coppersmith* [1994]. Morphotectonic evidence shows that the western part of the Trévaresse fold and thrust, now proposed as the source of the 1909 earthquake, is about 10 km-long. This leads us to hypothesize a rupture plane of 10 x

6.0-6.5 km that would require a coseismic slip of 0.5-0.6 m to match the observed seismic moment. This estimates' internal consistency is suggested also by simple scaling relationships and comparison with similarly large worldwide reverse faulting events.

As discussed earlier (see §2.), no seismic information exists on the subsurface of the Trévaresse fold, and even its deep structure and geometry of its thrust ramp are debated. Our focal mechanism tests, however, favor solutions with a high-angle fault dip (60°). Combining this finding with the hypothesized fault width (6.0-6.5 km) suggests that the rupture (1) is confined downward by the 6 km-deep "décollement" outlined in *Champion et al.* [2000], and (2) does not extend above 1 km depth, consistent with no surface breaks. Recall that 6 km is also the depth of the sole thrust underlying the Lubéron, the largest anticline of the region located about 20 km north of the study area (Figure 1, 2).

A further strong constraint from the seismological analysis of the 1909 earthquake is the need for a right-lateral component of slip. The Lambesc source is therefore a reverse fault with a right-lateral component, although a 135˚ estimate of the rake should probably be regarded as an upper boundary for the right-lateral component of motion.

To summarize this scenario, we inferred that the 1909 earthquake was caused by 0.5-0.6 m slip on a 10 x 6 km fault plane. This plane extends from 6.2 to 1.0 km depth beneath the westernmost segment of the Trévaresse fold and is aligned with it (strike=290˚). The steep northward dip of the fault (60˚) suggests that the rupture nucleated around 6 km depth near the major "décollement" of southern Provence. Our last step is to verify the consistency of this scenario against elevation changes resulting from a resurvey of the region around Lambesc.

6. Modeling of coseismic ground displacement

6.1. The leveling data: characteristics and limitations

Immediately after the 1909 earthquake, the French *Service de Nivellement Général* (SNG) resurveyed 464 km of first to fourth order leveling lines throughout and around the region that suffered the largest shaking effects. The results of the survey were presented to the French Academy of Sciences by Charles Lallemand [*Lallemand*, 1911], who had just gained valuable experience from a similar survey in the region after the 28 December 1908, Messina Straits, southern Italy, earthquake (Figure 15). Recently, *Romieu* [1994] and *Romieu et al.* [1998] reconsidered each individual geodetic line in this dataset. Quite surprisingly, both the original survey and its reinterpretation show elevation changes that do not taper to zero away from the epicentral area but remain quite significant. Obviously, this behavior can not be accounted for by coseismic displacement due to a buried fault. Two explanations are possible. First, there may be a substantial yet unexplored regional component of vertical displacement, which would imply progressive lowering of Provence at rates on the order of 0.5-1.0 mm/y. Or, there are important and systematic errors in the acquisition or in processing of some leveling lines, and particularly in assessing a common baseline for all of them. According to *Romieu* [1994], however, the main vertical motions observed between 1860-1969 are concentrated around the region of the Lambesc earthquake. This suggests that (1) insignificant regional signals can be removed rather easily, since they induce a constant offset throughout the entire region, and (2) a scenario of major uncertainties in the leveling lines or their processing is very likely.

Because the original data of *Lallemand* [1911] and *Romieu* [1994] are unavailable, we reconstructed the location of the original leveling lines with a twofold procedure: (1) for routes not modified after 1909, we used current benchmark locations supplied by the French National Geographic Institute (IGN); (2) for routes abandoned and reestablished along

different paths, we resorted to original drawings, 1/25,000 topographic maps and aerial photographs. Typical uncertainties are on the order of 0.1 and 0.5 km, respectively, for case (1) and (2).

Similarly, we had to infer the measured vertical displacements following a graphical procedure. From *Lallemand*'s [1911] original data, we retained the value read off the map at the corresponding distance along the given leveling line, with an expected uncertainty of ±0.5 km along the route. Concerning *Romieu*'s [1994] computations, we derived displacement values directly from the artwork illustrating his paper. In this case the expected error is ±0.1 mm for the elevation changes and ±0.05 km for distance along the leveling route.

6.2. Elastic dislocation modeling

Modeling was performed using *LandForms 1.8*, a Fortran code developed by G. Valensise and based on simple elastic dislocation in a homogeneous halfspace. Unlike most codes for dislocation modeling, *LandForms* subdivides the fault plane into smaller sub-faults (usually 1x1 km), a subdivision which helps obtain a smoother solution and may prevent singularities near the surface projection of the fault plane.

Based on the scenario from the previous section, we predicted the elevation changes associated with motion on a blind reverse fault located beneath the western portion of the Trévaresse anticline (Figure 16). The vertical displacement is also computed along the historical leveling lines shown in Figure 17 and compared with the elevation changes reported by *Lallemand* [1911] and re-evaluated by *Romieu* [1994]. The maximum uplift we obtained slightly exceeds 18 cm and the largest subsidence stays below 5 cm.

Given the characteristics of the 1909 source, the limited amount of slip, the substantial right-lateral component of motion, and the fact that the fault is almost certainly blind, we did not expect significant coseismic elevation changes following the Lambesc earthquake. This

expectation agrees with the limited vertical displacements obtained both by *Lallemand* [1911] and *Romieu* [1994]. Our calculations show that vertical displacements from the Lambesc earthquake source concentrate in the area of greatest damage. For this reason we compared our predictions only with the observations taken from geodetic routes for which our model predicts resolvable elevation changes, i.e. more than 1 mm (compare Figure 15 with Figure 16, 17). In other words, we make this comparison only for routes crossing the epicentral region, although these are third and fourth order. Unfortunately, the first and second order routes are farther from the region of interest. Furthermore, they must contain either (1) large survey or processing errors, or (2) non tectonic signals, or (3) tectonic signals not related to the 1909 earthquake. Whatever the relative importance of each of these unknown but potential contributions, it is just impossible to fit simultaneously the near- and far-field elevation changes by dislocation of a single fault, no matter how complicated the model is.

As shown in Figure 17, the general data trend is satisfactorily reproduced by our model fault. The same figure shows the relatively big difference between *Lallemand's* [1911] and *Romieu's* [1994] amplitudes coming from the same dataset and resulting from unknown differences in the data processing. Overall, the leveling data constrain rather tightly the fault's location (see the location of the uplifted zone along route C-D) and its steep dip (a more gentle dip would flip the subsidence zone from the south to the north flank of the Trévaresse, which would mean a severe misfit along route A-B). Unfortunately, the actual top depth of the fault is unconstrained, except for our observation that the displacement field is rather smooth in the transition zone between uplift and subsidence (see route A-B around St Cannat). This observation is consistent with the earthquake's limited size and with the lack of reported surface breaks.

7. Conclusions

We analyzed historical, seismological and geodetic observations of the 11 June 1909, Lambesc, southern France earthquake. Although the resolution of each of the individual datasets is rather limited, the joint analysis of such diverse datasets returned a robust solution.

The magnitude range of this earthquake was substantially narrowed (M_e 5.8, M_W 6.0 and M_S 6.0) and moved downward with respect to previous seismological estimates. Our preferred estimate of 6.0 corresponds to a relatively small fault area of ~65 km^2. The combination of macroseismic, geodetic and geologic observations suggests that the earthquake was generated by the western segment of the Trévaresse fold. Our best seismic source solution is a 10 x 6 km rupture plane oriented N290°, dipping 60° to the north and extending down to a depth of 6 km. This depth is similar to the "décollement" level of the Lubéron thrust, the main fold of the region. The focal mechanism exhibits a non-negligible right-lateral component of motion in addition to reverse motion. Finally, the analysis of source directivity suggests west-southwestward rupture propagation.

Seismological analyses also suggest that most of the moment was concentrated in the mainshock, which implies, given the estimated source length (10 km), that in 1909 the Trévaresse fold did not rupture its entire length (about 16 km). *Lacassin et al.* [2001] put forward the hypothesis that the eastern part of the fold ruptured during the largest aftershock of the sequence, about 31 minutes after the mainshock. Our analyses, however, reveal that this aftershock did not exceed magnitude 4.4, and was hence too small to support this hypothesis.

In conclusion, we believe that the fold's eastern portion did not rupture during the 1909 earthquake. Nevertheless, a reassessment of long-term elevation changes in western Provence by *Terrier* [1991] shows that a leveling line crossing the eastern tip of the fold just

east of Venelles (see Figure 16) recorded uplift coincident with the fold. This uplift does not appear in *Lallemand*'s [1911] original map (Figure 15) nor in *Romieu*'s [1994] reassessment. Although additional work is needed to pinpoint when deformation of this line occurred, the evidence from 1911 and 1994 could be interpreted as non-seismic motion of the eastern Trévaresse. The resulting scenario would be that only the western segment of the fold can generate significant earthquakes, and the eastern segment would have a dominantly creeping behavior.

It is encouraging to note that all results from the 1909 Lambesc earthquake are in good agreement with the region's tectonic and geodynamic framework. In particular, our preferred focal mechanism (P axis azimuth: 349°) agrees with the regional stress field obtained from focal mechanisms of relatively small earthquakes in southeastern France and the Ligurian Margin [*Baroux et al., 200*1a]. Furthermore, very recent GPS observations in the Alpine Arc and Southeastern France confirm shortening of the western Alps and Provence in a N-S to NW-SE direction [*Nocquet*, 2002]. These observations suggest that the 1909 Lambesc earthquake is the result of a tectonic style that is currently being delineated in some detail. Our work shows that this earthquake did not occur on a "new" fault but rather on an established and well known tectonic feature. This finding suggests that careful tectonic and geodynamic analyses aided by GPS data should have the capacity to highlight the areas that are more likely to experience destructive earthquakes in southeastern France.

Acknowledgments

We wish to commend the scientists listed below for their generosity in allowing us to gather all seismograms used in this study: Dr Stefano Solarino (Chiavari), Dr Torild Van Eck (De Bilt), Dr Arantza Ugalde (Ebre), Dr Joachim Ritter (Goettingen), Prof Torsten Dahm (Hamburg), Dr Paul Henni (Kew), Dr Michael Korn (Leipzig), Dr Eberhard Schmedes (Munich), Dr Diethelm Kaiser (Potsdam, Jena), Prof Michel Cara (Strasbourg), Dr Conny Holmquist (Uppsala) and Dr Bruce Presgrave (BCIS catalogue). For the leveling data, we thank Cyril Romieu and Gilles Ménard, who permitted us to look at their computations, and Olivier Bellier and Thierry Dusquesnoy who introduce us to them. Special thanks are due to Thomas Braun for his help in the investigation of historical seismograms and Roberto Basili for help with dislocation modeling. We thank the staff of SISMOS Project (INGV) for access to their digitizers and computers and continuous technical support, and Kathleen Jackson for her precious comments on our English. Finally, we are grateful to two anonymous reviewers for their helpful comments.

References

Angot, A. Note sur le tremblement de terre du 11 juin 1909. *C.R. Acad. Sci. Paris, CXLVIII,* 1640-1641, 1909a.

Angot, A. Sur les tremblements de terre des 11 et 23 juin. *C.R. Acad. Sci. Paris, CXLIX,* 71-73, 1909b.

Angot, A. Le tremblement de terre du 11 juin 1909 dans le Sud-Est de la France. I – Enquête du Bureau Central Météorologique. *Ann. Géogr*., *103,* 8-15, 1910.

Baroux, E. Tectonique active en région à sismicité modérée : le cas de la Provence (France). Apport d'une approche pluridisciplinaire. *Unpublished PhD thesis,* Univiersity of Paris-Sud, France, 327pp, 2000.

Baroux, E., N. Béthoux, and O. Bellier, Analyses of the stress field in southeastern France from earthquake focal mechanisms, *Geophysical Journal International, 145* (2), 336-348, 2001a.

Baroux, E., G. Valensise, N. A. Pino, O. Scotti, M. Cushing, and O. Bellier, Modelling the 1909 Lambesc earthquake with geodetic, macroseismic and instrumental data: implications for seismic hazard in Provence (France). EGS2001-26th General Assembly, Nice, France, 25-30 March 2001, *Geophysical Research Abstracts*, *3*, 2001b.

Boschi, E., E. Guidoboni, G. Ferrari, D. Mariotti, G. Valensise, and P. Gasperini, Catalogue of Strong Italian Earthquakes from 461 B. C. to 1997, *Annali di Geofisica*, *43(4)*, 607-868, with Database on CD-ROM, 2000.

Bono, A., B. De Simoni, A. Megna, A. Nardi and B. Palombo, Sismos Project: recovering and reprocessing historical seismic data. *Seismological research letters*, *73* (2), 2002.

Cara, M., D. Rouland, E. Peterschmitt, and L. Trotignon, Historical instruments and seismognrams in Strasbourg. *Gerlands Beitr. Geophysik, 96* (5), 374-384, 1987.

Carbon, D., Pré-étude des indices de déformation récente des chaînons provençaux ayant une relation structurale avec la Faille de la Durance. *GEOTER*. NTIS, GTR/CEA/1096-60, 1996.

Champion, C., Choukroune, P., and Clauzon, P., La déformation post-Miocène en Provence occidentale. *Geodyn. Acta, 13***,** 67-85, 2000.

Chardon, D., Bellier, O., Nguyen, F., Garambois, S., Jongmans, D., Hermitte, D. and Sébrier, M., The Trévaresse ridge anticline and the geological boundary conditions of the 1909 Lambesc (Provence, France) earthquake. *Geophysical Research Abstracts, 5*, 08882, 2003.

Ferrari, G., and E. Guidoboni, Seismic scenarios and assessment of intensity: some criteria for the use of the MCS scale, *Annali di Geofisica, 43*(4), 707-720, 2000.

Gasperini, P., F. Bernardini, G. Valensise, and E. Boschi, Defining seismogenic sources from historical earthquake felt reports, *Bull. Seism. Soc. Am.*, *89*, 94-110, 1999.

Gasperini, P., and G. Ferrari, Stima dei parametri sintetici, in: E. Boschi et al. (Eds.), *Catalogo dei Forti Terremoti in Italia dal 461 a.C. al 1980,* ING-SGA publ., 96-111, 1995.

Gasperini, P., and G. Ferrari. Stima dei parametri sintetici: nuove elaborazioni, in: E. Boschi et al. (Eds.), *Catalogo dei Forti Terremoti in Italia dal 461 a.C. al 1990,* ING- SGA publ., 56-64, 1997.

Griot-Pommera, D. A., and O. Scotti, Estimating earthquake location and magnitude from French seismic intensity observations. EGS2001-26th General Assembly, Nice, France, 25-30 March 2001, *Geophysical Research Abstracts*, *3*, 2001.

Kennet, B.L.N., and E.R. Engdahl. Traveltime for global location and phase identification, *Geophys. J. Int., 105*, 429-465. 1991.

Karnik, V., Seismicity of the European Area - Part I. *Czechoslovak Acad Sci. Publ.*, *D. Reidel Publishing Comp.*, Dordrecht, The Netherlands, 364 pp., 1969.

Lacassin, R., P. Tapponnier, B. Meyer, and R. Armijo, Was the Trévaresse thrust the source of the 1909 Lambesc (Provence, France) earthquake? Historical and geomorphic evidence, *C. R. Acad des Sciences, Paris, TIIa, 333*, 571-581, 2001.

Lallemand, C., Sur les changements du niveau du sol en Provence, à la suite du tremblement de terre du 11 juin 1909. *C. R. Acad des Sciences, Paris, 152*, 1560-1562, 1911.

Lemoine, P. Le tremblement de terre du 11 juin 1909 dans le Sud-Est de la France. II - Observations sur place dans la région dévastée. *Ann. Géogr*., *103,* 15-25, 1910.

Levret, A., J. C. Backe, and M. Cushing, Atlas of macroseismic maps for French earthquakes with their principal characteristics. *Natural Hazards, 10***,** 19-46, 1994.

Levret, A., M. Cushing, and G. Peyridieu, Recherche des caractéristiques des séismes en France. Atlas de 140 cartes macrosismiques. Edited by IPSN, Fontenay-aux-Roses, France, 2 Vols., 1996.

Massinon, B., "Annexe". In *Les tremblements de Terre en France*. Edited by J. Vogt. 203-204. Mémoires du BRGM. *69*, 1979.

Medvedev, S. P., W. Sponheuer, and V. Karnik. Seismic intensity scale version 1964. *Inst. Geody. Publ.*, *48*, Jena, 1967.

Nocquet, J.M. Mesure de la déformation crustale en Europe occidentale par géodésie spatiale. *Unpublished PhD thesis*, University of Nice-Sophia-Antipolis, France. 2002.

Pino, N. A., D. Giardini, and E. Boschi, The December 28, 1908, Messina Straits, southern Italy, earthquake: waveform modeling of regional seismograms, *J. Geophys. Res., 105*, *B11* (25),473-25,492, 2000.

Romieu, C., Utilisation du nivellement pour caractériser la déformation actuelle en Provence Occidentale. *Unpublished master thesis*, Ecole Nationale des Sciences Géographiques, France, 1994.

Romieu, C., S Moine, and G. Ménard, Réévaluation des mouvements verticaux associés au séisme de Lambesc (Provence, 11 juin 1909). *MAST*. Les Houches, France, October 1998. *Ecole de Physique publ*., 1998.

Rothé, J. P., La sismicité des Alpes Occidentales, *Bull. Géol. France*, *5e série, T. II*, 295-320, 1942.

Sieberg, A., Erdebeben, in: B. Gutenberg (Ed.), *Handbuch der Geophysik*, *4*, 552-554, 1932.

SisFrance, Base de données national des séismes ressentis en France métropolitaine. *BRGM/EDF/IPSN Eds.,website* http://www.sisfrance.net/, 2000.

SISMOS Project in INGV web site. http://www.ingv.it/~roma/framesx/progetti/sismos/framewelcome.html

Spiess, Cdt. Note sur le tremblement de terre de Provence. *Proceedings of the French Congress of Scientific Societies - Comptes rendus du Congrès des Sociétés Savantes*. Paris. 1926.

Terrier, M., Néotectonique de la Provence Occidentale (France) : vers une analyse multicritère des déformations récentes. Application à la classification des structures sismogènes. *Phd Thesis - Doc BRGM*, Provence, University - Marseille, France, 1991.

Valensise, G., and D. Pantosti (eds), Database of Potential Sources for Earthquakes Larger than M 5.5 in Italy. *Annali di Geofisica*, *44* (4), Suppl., with full Database on CD-ROM (available in part also at http://www.ingv.it/), 2001.

Wells, D. L., and K. J. Coppersmith, New empirical relationships among magnitude, rupture length, rupture width, rupture area, and surface displacement, *Bull. Seism. Soc. Am., 84*, 974-1,002, 1994

Figure captions

Figure 1: Tectonic sketch of southeastern France showing historical and instrumental seismicity.

Figure 2: Map of intensity data for the 11 June 1909, Lambesc earthquake supplied by *SisFrance* [2000] and isoseismals from *Levret et al.* [1996]. Only intensities V and higher are shown (see Table 1 for the full list down to intensity IV). The solid and dotted boxes represent source models obtained using the *Boxer* code, respectively with the full dataset and after removal of two anomalous datapoints that are believed to reflect site amplifications (shown by black arrows). The cones represent the orientation uncertainty associated with each box. The solution shown with the solid box is our preferred source model; the star represents the corresponding epicenter. The SISFRANCE epicentral position, estimated by computing the barycentre of the highest degrees isoseismals, is coincident with the full dataset Boxer epicenter.

Figure 3: Diagram of the theoretical instrumental response for all the stations for which we digitized the original seismograms.

Figure 4: An example of an original historical seismogram recorded at Strasbourg; a) before processing, b) digitized and corrected.

Figure 5: Great circle paths from the 1909 earthquake source to the stations for which at least one seismogram for on component was available. Solid lines indicate stations for which both the surface wave magnitude M_S and the moment magnitude M_W were computed, while dashed

line and dash-dot line indicate station for which only M_S or M_W were estimated, respectively, for the corresponding station. The focal mechanism represents our preferred solution based on all available data and analyses. The dotted line indicates the raypath between the epicenter of the 13 April 1992 Roermond earthquake and the station SSB (Saint-Sauveur, France). We used seismograms of this earthquake to constrain the crustal model between the epicenter of the 1909 earthquake and the station De Bilt (DBN).

Figure 6: Azimuthal representation of the M_S computed from the Lambesc earthquake seismograms using the Prague formula. The segment length is proportional to the epicenter-station distance. N, E and Z indicate the three seismograph components. W and B respectively indicate that the seismograms were written by a Wiechert or Bosch instrument. See Tables 2 and 3 and text for further details.

Figure 7: Seismograms of the 1992 Roermond earthquake recorded at SSB (St Sauveur, France) that were used to calibrate the crustal model for computing the seismic moment of the 1909 event. Solid lines correspond to the synthetic seismograms, dashed lines to the data.

Figure 8: Test of synthetic seismograms (solid line) obtained for widely different focal solutions (pure normal, pure reverse, pure strike-slip) against seismograms recorded in 1909 at GTT (Goettingen) and DBN (De Bilt, Bosch seismograph only). The upper portion of the figure shows the original data (Z, N and E components, respectively from left to right). The duration of each signal is 400 seconds. The data are also reported with dashed lines under each synthetic seismogram.

Figure 9: Test of synthetic seismograms (solid lines) obtained for 27 hypothetical sets of focal parameters selected around our preferred model fault. The 27 solutions are compared

with the seismograms recorded in 1909 at GTT. The original signals for the Z, N and E components are shown in the upper portion of the figure. The duration of each signal is 400 seconds. The data are also reported with dashed lines under each synthetic seismogram.

Figure 10: Test of synthetic seismograms (solid lines) obtained for 27 hypothetical sets of focal parameters selected around our preferred model fault. The 27 solutions are compared with the seismograms recorded in 1909 at DBN (Bosch seismograph). The original signals for the N and E components are shown in the upper portion of the figure. The duration of each signal is 400 seconds. The data are also reported with dashed lines under each synthetic seismogram.

Figure 11: Comparison between data (dashed line) and synthetics (solid line) predicted by using the source focal mechanism corresponding to #27 in Figures 9 and 10. The reported seismic moment is obtained by matching the amplitude of the main arrivals. For VIE the seismic moment is to be considered a minimum value.

Figure 12: Variability of magnitude (Y-axis) vs. the angle formed between fault strike and the observer (on the X-axis). The solid line represents the surface wave magnitude M_S, the dashed line the moment magnitude M_W. The dotted line connects M_W values corrected for the effect of directivity.

Figure 13: S waveforms recorded by the Bosch instrument at De Bilt (DBN) and by the Wiechert instrument at Gottingen (GTT). Even though the natural period of the pendula of the two instruments is very similar, the duration of the pulses appears rather different.

Figure 14: Comparison between data (bottom) and synthetic waveforms for the horizontal components at Ebre (EBR), computed using different triangular source time functions (5 s, 2 s, 1 s). All waveforms shown here are unfiltered.

Figure 15: Map of earthquake damage and elevation changes measured by *Lallemand* [1911] following the 1909 earthquake. A: original figure, B: redrawn. Key: (1, dark gray) area of partial or total collapse of buildings; (2, medium gray) area that suffered large and extensive cracks in walls, collapse of chimneys and fall of pieces of plaster; (3, light gray) area where objects fell down from shelves; (4, white) area where the bells rang, clocks stopped, hanging objects like chandeliers swung.

Leveling lines are shown as follows: (5, dashed line) 1st and 2nd order; (6, dotted line) 3rd and 4th order. Contours of observed vertical displacement (7 & 8) are expressed in centimeters. Notice that some of the contours are open towards regions located away from the meizoseismal area (e.g., towards the northeast and southeast), suggesting that either the data require additional processing to adjust the respective baselines, or the measured strain field reflects regional signals not related with the 1909 earthquake, or a combination of the two.

Figure 16: Map of coseismic elevation changes (solid lines) expected to result from slip along the model fault obtained from macroseismic and seismographic analyses and from geological constraints described in §5. Contour interval is 2 mm. Observed and expected displacements along the leveling routes A-B and C-D are shown in Figure 17.

Figure 17: The upper boxes show observed and expected displacement along selected leveling routes crossing the Lambesc region (see Figure 16 for location): the dotted lines represent the original geodetic data of *Lallemand* [1911]; the dashed lines show the data reappraisal reported by *Romieu* [1994]; the solid lines show the expected coseismic

displacement due to slip along the 60˚-dipping model fault described in §5. The lower boxes show the general trend of topography along the route and the spatial relationships with the model fault.

Table captions

Table 1: List of all intensities IV-V and higher observed following the 11 June 1909, Lambesc earthquake (from the *SisFrance Database* [2000]). The two datapoints that were removed because of site amplification effects are shown in Italic.

Table 2: Characteristics of the different historical seismographs; for each station the table supplies also the distance (in km and degrees) and the azimuth with respect to the epicenter of the 1909 Lambesc earthquake.

Table 3: Moment magnitude and surface wave magnitude obtained from each seismogram. Field *D* supplies the epicentral distance in km and degrees for each station. Field M_S shows the magnitude corrected for the characteristic period (given in field *T*) of the largest amplitude pulse following *Karnik* [1969].

Table 4: Surface wave magnitudes obtained for a few seismograms for the largest aftershock of the 1909 Lambesc earthquake. The GTT measurement comes a recording written by the 17 tons Weichert instrument. The amplitude and period of surface waves was obtained from the station bulletin (B) or directly read on the seismogram (S). For characteristics of the station and of the instrument see Tables 2 and 3.

Table 1: List of all intensities IV-V and higher observed following the 11 June 1909, Lambesc earthquake (from the *SisFrance Database* [2000]). The two datapoints that were removed because of site amplification effects are shown in Italic.

Lon	Lat	Int	Locality
5.35	*43.67*	*IX*	*VIEUX-ROGNES (ROGNES)*
5.27	43.65	VIII-IX	LAMBESC
5.30	43.62	VIII-IX	SAINT-CANNAT
5.17	*43.68*	*VIII-IX*	*VERNEGUES*
5.43	43.67	VIII	LE PUY-SAINTE-REPARADE
5.48	43.60	VIII	VENELLES
6.55	43.62	VII	BARGEMON
5.25	43.72	VII	CHARLEVAL
5.07	43.57	VII	CORNILLON-CONFOUX
5.18	43.63	VII	LA BARBEN
5.32	43.72	VII	LA ROQUE-D'ANTHERON
5.15	43.63	VII	PELISSANNE
5.50	43.70	VII	PERTUIS
5.43	43.58	VII	PUYRICARD (AIX-EN-PROVENCE)
5.35	43.67	VII	ROGNES
5.10	43.65	VII	SALON-DE-PROVENCE
5.45	43.53	VI-VII	AIX-EN-PROVENCE
5.17	43.70	VI-VII	ALLEINS
5.47	43.73	VI-VII	ANSOUIS
5.15	43.67	VI-VII	AURONS
5.35	43.57	VI-VII	EGUILLES
5.03	43.70	VI-VII	EYGUIERES
5.58	43.77	VI-VII	GRAMBOIS
5.07	43.62	VI-VII	GRANS
5.13	43.58	VI-VII	LANCON-PROVENCE
5.32	43.75	VI-VII	LAURIS
5.37	43.77	VI-VII	LOURMARIN
5.18	43.73	VI-VII	MALLEMORT
5.53	43.63	VI-VII	MEYRARGUES
5.58	43.65	VI-VII	PEYROLLES-EN-PROVENCE
5.23	43.75	VI-VII	PUGET
5.35	43.77	VI-VII	PUYVERT
5.40	43.68	VI-VII	SAINT-ESTEVE-JANSON
4.72	43.42	VI-VII	SALIN-DE-GIRAUD (ARLES)
5.93	43.13	VI-VII	TOULON
5.30	43.53	VI-VII	VENTABREN
5.43	43.72	VI-VII	VILLELAURE
3.47	43.32	VI	AGDE
5.57	43.30	VI	AUBAGNE
4.95	43.72	VI	AUREILLE
4.82	43.95	VI	AVIGNON
7.08	44.30	VI	BAGNI DI VINADIO
4.90	44.03	VI	BEDARRIDES
5.38	43.73	VI	CADENET
5.53	43.22	VI	CASSIS
4.85	43.88	VI	CHATEAURENARD
4.48	43.95	VI	COLLIAS
4.98	43.52	VI	ISTRES
5.63	43.63	VI	JOUQUES
5.63	43.78	VI	LA BASTIDE-DES-JOURDANS
5.57	43.70	VI	LA BASTIDONNE
5.20	43.55	VI	LA FARE-LES-OLIVIERS
5.52	43.28	VI	LA PENNE-SUR-HUVEAUNE
5.55	43.73	VI	LA TOUR-D'AIGUES
5.08	43.70	VI	LAMANON
5.40	43.28	VI	MARSEILLE
5.20	43.75	VI	MERINDOL
5.50	43.48	VI	MEYREUIL
5.65	43.70	VI	MIRABEAU
5.00	43.58	VI	MIRAMAS
4.60	43.88	VI	MONTFRIN
3.87	43.62	VI	MONTPELLIER
4.87	43.68	VI	MOURIES
4.50	43.83	VI	REDESSAN
5.62	43.48	VI	ROUSSET
5.03	43.55	VI	SAINT-CHAMAS
4.43	43.68	VI	SAINT-GILLES
5.52	43.55	VI	SAINT-MARC-JAUMEGARDE
6.77	43.43	VI	SAINT-RAPHAEL
5.08	43.75	VI	SENAS
3.70	43.40	VI	SETE
5.60	43.55	VI	VAUVENARGUES
4.20	43.57	V-VI	AIGUES-MORTES
5.68	43.73	V-VI	BEAUMONT-DE-PERTUIS
5.55	43.52	V-VI	BEAURECUEIL
3.22	43.35	V-VI	BEZIERS
7.02	43.57	V-VI	CANNES
5.10	44.12	V-VI	CAROMB
5.57	43.48	V-VI	CHATEAUNEUF-LE-ROUGE
7.73	43.82	V-VI	COLDIRODI
5.43	43.77	V-VI	CUCURON
6.47	43.53	V-VI	DRAGUIGNAN
3.25	43.57	V-VI	FOS
3.98	44.08	V-VI	GENERARGUES
6.05	43.17	V-VI	LA FARLEDE
5.88	43.10	V-VI	LA SEYNE-SUR-MER
5.52	43.52	V-VI	LE THOLONET
5.20	43.83	V-VI	MENERBES
7.27	43.70	V-VI	NICE
4.37	43.83	V-VI	NIMES
8.03	43.88	V-VI	ONEGLIA
4.57	43.93	V-VI	REMOULINS
5.62	43.25	V-VI	ROQUEFORT-LA-BEDOULE
5.58	43.52	V-VI	SAINT-ANTONIN-SUR-BAYON
5.72	43.68	V-VI	SAINT-PAUL-LES-DURANCE
5.48	43.75	V-VI	SANNES
4.70	44.02	V-VI	TAVEL
6.48	43.50	V-VI	TRANS-EN-PROVENCE
4.42	44.02	V-VI	UZES
4.63	43.85	V-VI	VALLABREGUES
5.42	43.78	V-VI	VAUGINES
8.17	44.00	V	ALASSIO
5.40	43.88	V	APT
4.63	43.68	V	ARLES
5.03	44.10	V	AUBIGNAN
5.47	43.83	V	AURIBEAU
5.17	43.48	V	BERRE-L'ETANG
5.32	43.82	V	BONNIEUX
7.65	43.77	V	BORDIGHERA
5.38	43.83	V	BUOUX
5.50	43.78	V	CABRIERES-D'AIGUES
5.48	43.83	V	CASTELLET
4.95	43.90	V	CAUMONT-SUR-DURANCE
5.03	43.83	V	CAVAILLON
5.75	43.77	V	CORBIERES
6.07	43.23	V	CUERS
7.62	43.85	V	DOLCEACQUA

7.80	44.28	V	FRABOSA SOPRANA
5.57	43.45	V	FUVEAU
5.47	43.45	V	GARDANNE
5.37	43.90	V	GARGAS
5.85	43.67	V	GINASSERVIS
5.20	43.92	V	GORDES
5.25	43.87	V	GOULT
6.92	43.67	V	GRASSE
6.13	43.12	V	HYERES
5.05	43.92	V	L'ISLE-SUR-LA-SORGUE
5.60	43.18	V	LA CIOTAT
5.52	43.77	V	LA MOTTE-D'AIGUES
4.23	43.93	V	LA ROUVIERE
5.28	43.83	V	LACOSTE
4.28	44.53	V	LARGENTIERE
3.75	44.37	V	LE PONT-DE-MONTVERT
5.00	43.93	V	LE THOR
4.80	43.75	V	LES BAUX-DE-PROVENCE
5.78	43.83	V	MANOSQUE
5.13	43.85	V	MAUBEC
5.13	44.05	V	MAZAN
4.95	43.80	V	MOLLEGES
4.75	44.55	V	MONTELIMAR
5.00	44.03	V	MONTEUX
6.07	43.65	V	MONTMEYAN
5.78	43.37	V	NANS-LES-PINS
5.85	43.13	V	OLLIOULES
5.03	43.78	V	ORGON
3.93	43.53	V	PALAVAS-LES-FLOTS
4.78	43.72	V	PARADOU
5.05	44.00	V	PERNES-LES-FONTAINES
2.90	42.70	V	PERPIGNAN
5.57	43.78	V	PEYPIN-D'AIGUES
3.77	43.58	V	PIGNAN
5.00	43.82	V	PLAN-D'ORGON
4.82	43.38	V	PORT-SAINT-LOUIS-DU-RHONE
5.68	43.53	V	PUYLOUBIER
6.03	43.70	V	QUINSON
5.77	43.60	V	RIANS
4.20	44.50	V	RIBES
2.87	42.77	V	RIVESALTES
5.12	43.85	V	ROBION
5.43	43.87	V	SAIGNON
5.93	43.08	V	SAINT-MANDRIER-SUR-MER
5.52	43.87	V	SAINT-MARTIN-DE-CASTILLON
5.53	43.77	V	SAINT-MARTIN-DE-LA-BRASQUE
5.72	43.92	V	SAINT-MICHEL-L'OBSERVATOIRE
5.22	43.88	V	SAINT-PANTALEON
4.83	43.78	V	SAINT-REMY-DE-PROVENCE
5.53	43.40	V	SAINT-SAVOURNIN
5.77	43.78	V	SAINTE-TULLE
7.90	43.83	V	SAN STEFANO A MARE
5.40	43.83	V	SIVERGUES
7.85	43.87	V	TAGGIA
5.08	43.83	V	TAILLADES
4.90	44.18	V	TRAVAILLAN
5.25	43.52	V	VELAUX
5.15	44.00	V	VENASQUE
7.60	43.78	V	VENTIMIGLIA
4.22	43.75	V	VERGEZE
5.57	43.90	V	VIENS
4.60	44.75	V	VILLENEUVE (COUX)
8.22	44.05	IV-V	ALBENGA
4.68	43.88	IV-V	ARAMON
7.77	43.88	IV-V	CERIANA
4.95	43.93	IV-V	CHATEAUNEUF-DE-GADAGNE
4.95	43.77	IV-V	EYGALIERES
5.23	43.40	IV-V	GIGNAC-LA-NERTHE
4.93	43.95	IV-V	JONQUERETTES
4.23	44.48	IV-V	JOYEUSE
8.15	43.97	IV-V	LAIGUEGLIA
5.30	43.95	IV-V	LIOUX
4.78	43.83	IV-V	MAILLANE
5.05	43.40	IV-V	MARTIGUES
3.50	44.52	IV-V	MENDE
7.82	44.38	IV-V	MONDOVI
5.70	43.83	IV-V	MONTFURON
5.63	43.45	IV-V	PEYNIER
5.75	43.82	IV-V	PIERREVERT
4.38	44.62	IV-V	PONT-D'AUBENAS (AUBENAS)
4.98	43.42	IV-V	PORT-DE-BOUC
4.80	43.90	IV-V	ROGNONAS
4.95	43.83	IV-V	SAINT-ANDIOL
4.93	43.95	IV-V	SAINT-SATURNIN-LES-AVIGNON
5.43	43.43	IV-V	SIMIANE-COLLONGUE

Table 2: Characteristics of the different historical seismographs; for each station the table supplies also the distance (in km and degrees) and the azimuth with respect to the epicenter of the 1909 Lambesc earthquake

	Code	Station	Latitude	Longitude	Seismometer	Comp	Mass (kg)	Period (s)	Magnif.	Damping	Δ (°)	Dist. (km)	Azimuth	Ms	Digit.	Mw
1	DBN	De Bilt (NL)	52.1017	5.1767	WIECHERT	E-W	1000?	4.9-5.2	170-177	0.4	8.45	940	359	Yes	Yes	Yes
2	DBN	De Bilt (NL)	52.1017	5.1767	WIECHERT	N-S	1000?	4.9-5.2	157-161	0.4	8.45	940	359	Yes	Yes	Yes
3	DBN	De Bilt (NL)	52.1017	5.1767	BOSCH	E-W	1000?	17.9-18.0	20.1-20.3	0.4	8.45	940	359	Yes	Yes	Yes
4	DBN	De Bilt (NL)	52.1017	5.1767	BOSCH	N-S	1000?	18.1-18.2	20.2-20.6	0.4	8.45	940	359	Yes	Yes	Yes
5	EBR	Ebre (SP)	40.820556	0.493889	VICENTINI	E-W	100	2.3	90		4.46	496.2	235	No	Yes	No
6	EBR	Ebre (SP)	40.820556	0.493889	VICENTINI	N-S	100	2.3	90		4.46	496.2	235	No	Yes	No
7	GTT	Goettigen (D)	51.5464	9.9642	WIECHERT	N-S	1200	11.7	147	0.35	8.66	961.9	20	Yes	Yes	Yes
8	GTT	Goettigen (D)	51.5464	9.9642	WIECHERT	E-W	1200	11.7	157	0.4	8.66	961.9	20	Yes	Yes	Yes
9	GTT	Goettigen (D)	51.5464	9.9642	WIECHERT	Z	1200	5.7	159	0.55	8.66	961.9	20	Yes	Yes	Yes
10	GTT	Goettigen (D)	51.5464	9.9642	WIECHERT	N-S	17000	1.41	2220	0.52	8.66	961.9	20	Yes	No	No
11	HAM	Hamburg (D)	53.55931	9.98108	WIECHERT	N-S	1000	10	195	0.48	10.54	1171.6	15	Yes	Yes	Yes
12	LEI	Leipzig (D)	51.335	12.3916	WIECHERT	E-W		8.5	241	0.268	9.20	1022.2	28.9	Yes	Yes	Yes
13	LEI	Leipzig (D)	51.335	12.3916	WIECHERT	N-S		8.5	227	0.335	9.20	1022.2	28.9	Yes	Yes	Yes
14	MNH	Munich (D)	48.1461	11.6089	WIECHERT	E-W	1000	12.5	230	0.46	6.41	712	41.1	Yes	No	No
15	PAR	Paris-St Maur (F)	48.836389	2.3375	WIECHERT	E-W	200	8	80	1.0 (*)	5.74	637.8	340	Yes	Yes	Yes
16	POT	Potsdam (D)	52.3803	13.0678	WIECHERT	E-W	1000	14	130	0.48	10.3	1144	27.5	Yes	Yes	Yes
17	POT	Potsdam (D)	52.3803	13.0678	WIECHERT	N-S	1000	14	133	0.48	10.3	1144	27.5	Yes	Yes	Yes
18	STR	Strasbourg (F)	48.583	7.7694	WIECHERT	N-S	1000	10	230	0.35	5.38	597.7	18	Yes	Yes	Yes
19	UPP	Uppsala (S)	59.8581	17.6256	WIECHERT	N-S		9.2	187	0.385	18.0	2003.0	20.3	Yes	Yes	Yes
20	UPP	Uppsala (S)	59.8581	17.6256	WIECHERT	E-W		9.2	187	0.385	18.0	2003.0	20.3	Yes	Yes	Yes
21	VIE	Vienna (A)	48.25	16.3583	WIECHERT	N-S	1000	10.9	160	0.2	9.06	1006	54.4	Yes	Yes	Yes
22	VIE	Vienna (A)	48.25	16.3583	WIECHERT	E-W	1000	11.5	165	0.2	9.06	1006	54.4	Yes	Yes	Yes

Table 3: Moment magnitude and surface wave magnitude obtained from each seismogram. Field *D* supplies the epicentral distance in km and degrees for each station. Field M_S shows the magnitude corrected for the characteristic period (given in field *T*) of the largest amplitude pulse following *Karnik* [1969].

	Code	Station	Comp.	Ms	T(s)	Mo (N.m)	Mw	D (°)	D (km)	Azimuth	Lat	Long	Seismometer
1	DBN	De Bilt (NL)	N-S	***6.41***	7.8	2.50E+18	***6.2***	8.45	940	359	52.10170	5.17670	Wiechert
2	DBN	De Bilt (NL)	E-W	***6.42***	8.1	2.50E+18	***6.2***	8.45	940	359	52.10170	5.17670	Wiechert
3	DBN	De Bilt (NL)	N-S	***6.08***	9.6	1.50E+18	***6.05***	8.45	940	359	52.10170	5.17670	Bosch
4	DBN	De Bilt (NL)	E-W	***5.93***	17.6	1.10E+18	***5.96***	8.45	940	359	52.10170	5.17670	Bosch
5	GTT	Goettigen (D)	Z	***5.74***	5.5	1.20E+17	***5.32***	8.66	961.9	20	51.54640	9.96420	Wiechert
6	GTT	Goettigen (D)	N-S	***5.8***	9.1	3.00E+17	***5.58***	8.66	961.9	20	51.54640	9.96420	Wiechert
7	GTT	Goettigen (D)	E-W	***5.96***	12	2.30E+17	***5.51***	8.66	961.9	20	51.54640	9.96420	Wiechert
8	GTT	Goettigen (D)	N-S	***5.78***	2			8.66	961.9	20	51.54640	9.96420	Wiechert
9	HAM	Hambourg (D)	N-S	***6.02***	7	7.00E+17	***5.83***	10.54	1171.6	15	53.55931	9.98108	Wiechert
10	LEI	Leipzig (D)	N-S	***5.66***	10	1.70E+17	***5.42***	9.20	1022.2	28.9	51.33500	12.39160	Wiechert
11	LEI	Leipzig (D)	E-W	***5.7***	8	1.00E+17	***5.27***	9.20	1022.2	28.9	51.33500	12.39160	Wiechert
12	MNH	Munich (D)	N-S	***5.93***	5.5			6.41	712	41.1	48.14610	11.60890	Wiechert
13	PAR	Paris - St Maur (F)	E-W	***6.33***	3.8	1.40E+18	***6.03***	5.74	637	340	48.83639	2.33750	Wiechert
14	POT	Potsdam (D)	N-S	***6.19***	3.8	5.00E+17	***5.73***	10.3	1144	27.5	52.38030	13.06780	Wiechert
15	POT	Potsdam (D)	E-W	***6.12***	6	2.00E+17	***5.47***	10.3	1144	27.5	52.38030	13.06780	Wiechert
16	STR	Strasbourg (F)	N-S	***6.08***	5.8	5.00E+17	***5.73***	5.38	597.7	18	48.58300	7.76940	Wiechert
17	UPP	Uppsala (S)	N-S	***5.44***	13.8	7.00E+16	***5.16***	18.0	2003.0	20.3	59.85810	17.62560	Wiechert
18	UPP	Uppsala (S)	E-W	***5.58***	7.3	7.00E+16	***5.16***	18.0	2003.0	20.3	59.85810	17.62560	Wiechert
19	VIE	Vienna (A)*	N-S	***5.65-5.86***	7.6	1E+17-1.62E+17	***5.27-5.4****	9.06	1006.0	54.0	48.25	16.3583	Wiechert
20	VIE	Vienna (A)*	E-W	***5.72-5.93***	6.3	1E+17-1.62E+17	***5.27-5.4****	9.06	1006.0	54.0	48.25	16.3583	Wiechert

*: see text (§4) for details

Table 4: Surface wave magnitudes obtained for a few seismograms for the largest aftershock of the 1909 Lambesc earthquake. The GTT measurement comes a recording written by the 17 tons Weichert instrument. The amplitude and period of surface waves was obtained from the station bulletin (B) or directly read on the seismogram (S). For characteristics of the station and of the instrument see Tables 2 and 3.

	Code	Station	Comp.	Ms	T(s)	Kind
1	DBN	De Bilt (NL)	N-S	***4.5***	4	B&S
2	DBN	De Bilt (NL)	E-W	***4.5***	4	B&S
3	GTT	Goettigen (D)	N-S	***4.4***	1.4	S
4	HAM	Hambourg (D)	N-S	***4.2***	9	B
5	HAM	Hambourg (D)	E-W	***4.4***	9	B
6	LEI	Leipzig (D)	N-S	***4.3***	4	B
7	LEI	Leipzig (D)	E-W	***4.3***	4	B

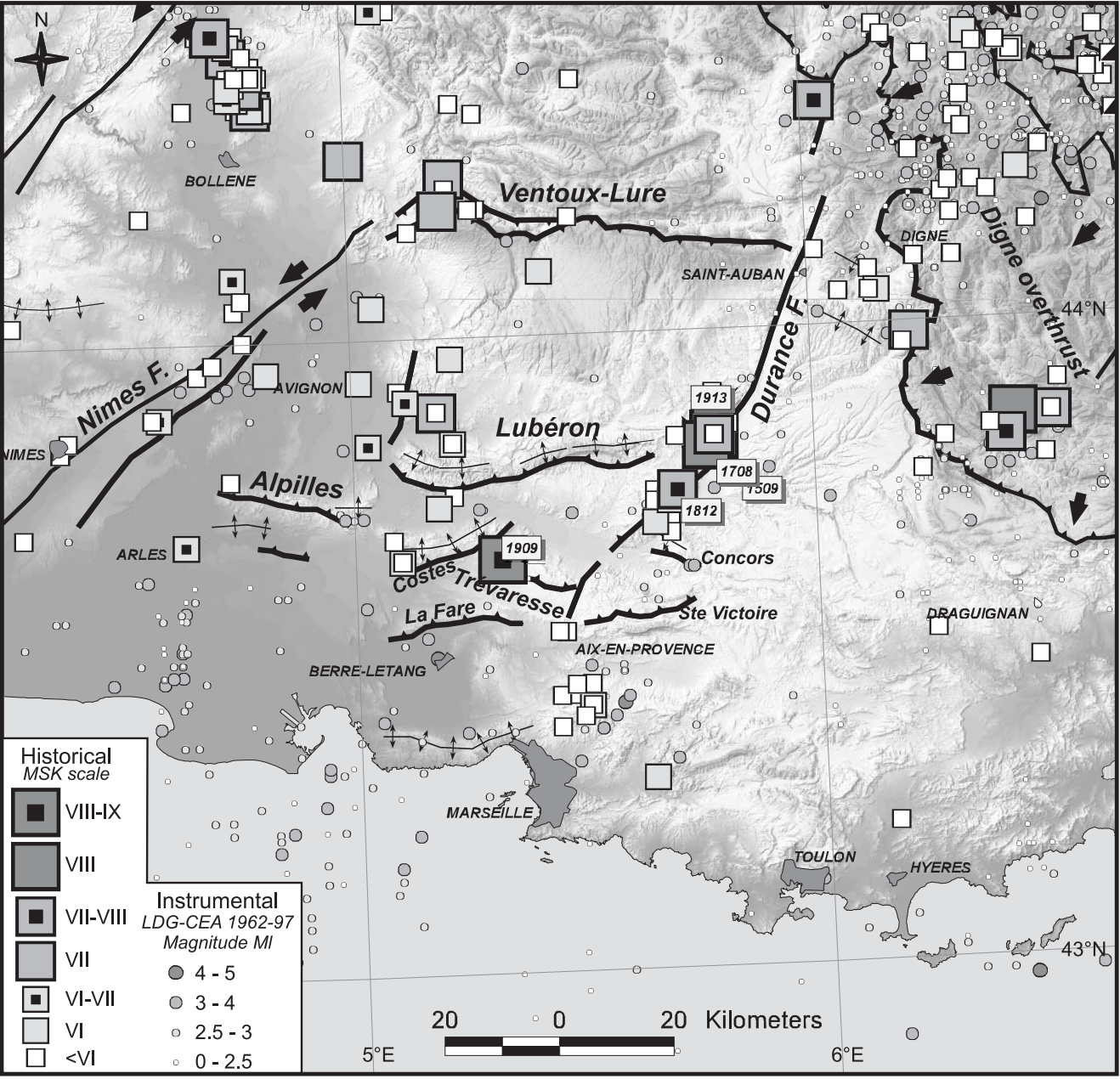
N
BOLLENE
Ventoux-Lure
SAINT-AUBAN
DIGNE
Digne overthrust
Durance F.
44°N
Nimes F.
AVIGNON
NIMES
Lubéron
1913
1708
1509
1812
Alpilles
ARLES
1909
Concors
Costes Trévaresse
La Fare
Ste Victoire
DRAGUIGNAN
AIX-EN-PROVENCE
BERRE-LETANG
MARSEILLE
TOULON
HYERES
43°N
Historical
MSK scale
VIII-IX
VIII
VII-VIII
VII
VI-VII
VI
<VI
Instrumental
LDG-CEA 1962-97
Magnitude Ml
4 - 5
3 - 4
2.5 - 3
0 - 2.5
20 0 20 Kilometers
5°E
6°E

Figure 1

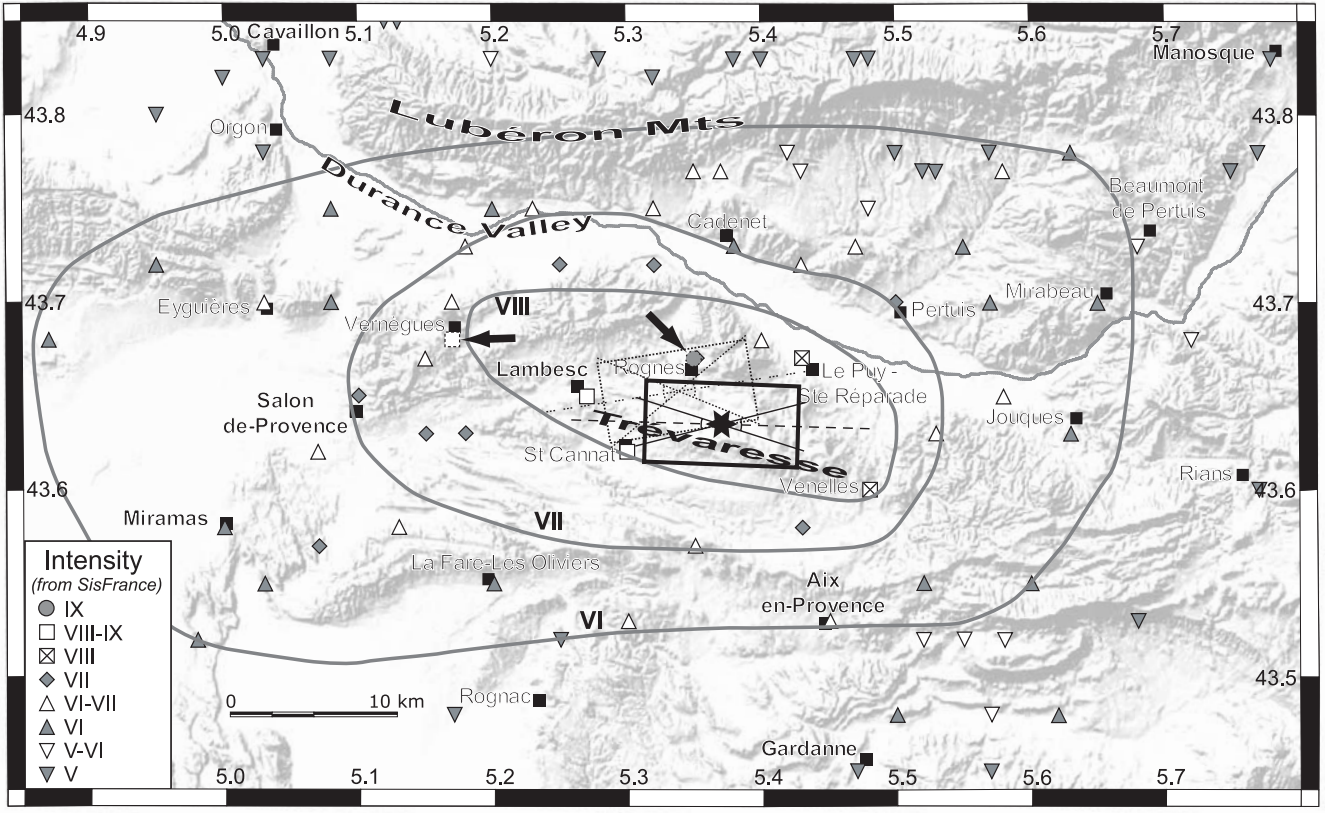
4.9
5.0
5.1
5.2
5.3
5.4
5.5
5.6
5.7
43.8
43.7
43.6
43.5
Cavaillon
Manosque
Orgon
Lubéron Mts
Durance Valley
Cadenet
Beaumont de Pertuis
Eyguières
Vernègues
VIII
Pertuis
Mirabeau
Lambesc
Rognes
Le Puy - Ste Réparade
Salon de-Provence
Jouques
Fréyaresse
St Cannat
Venelles
Rians
Miramas
VII
La Farc-Les Oliviers
Aix en-Provence
VI
0
10 km
Rognac
Gardanne
Intensity
(from SisFrance)
IX
VIII-IX
VIII
VII
VI-VII
VI
V-VI
V

Figure 2

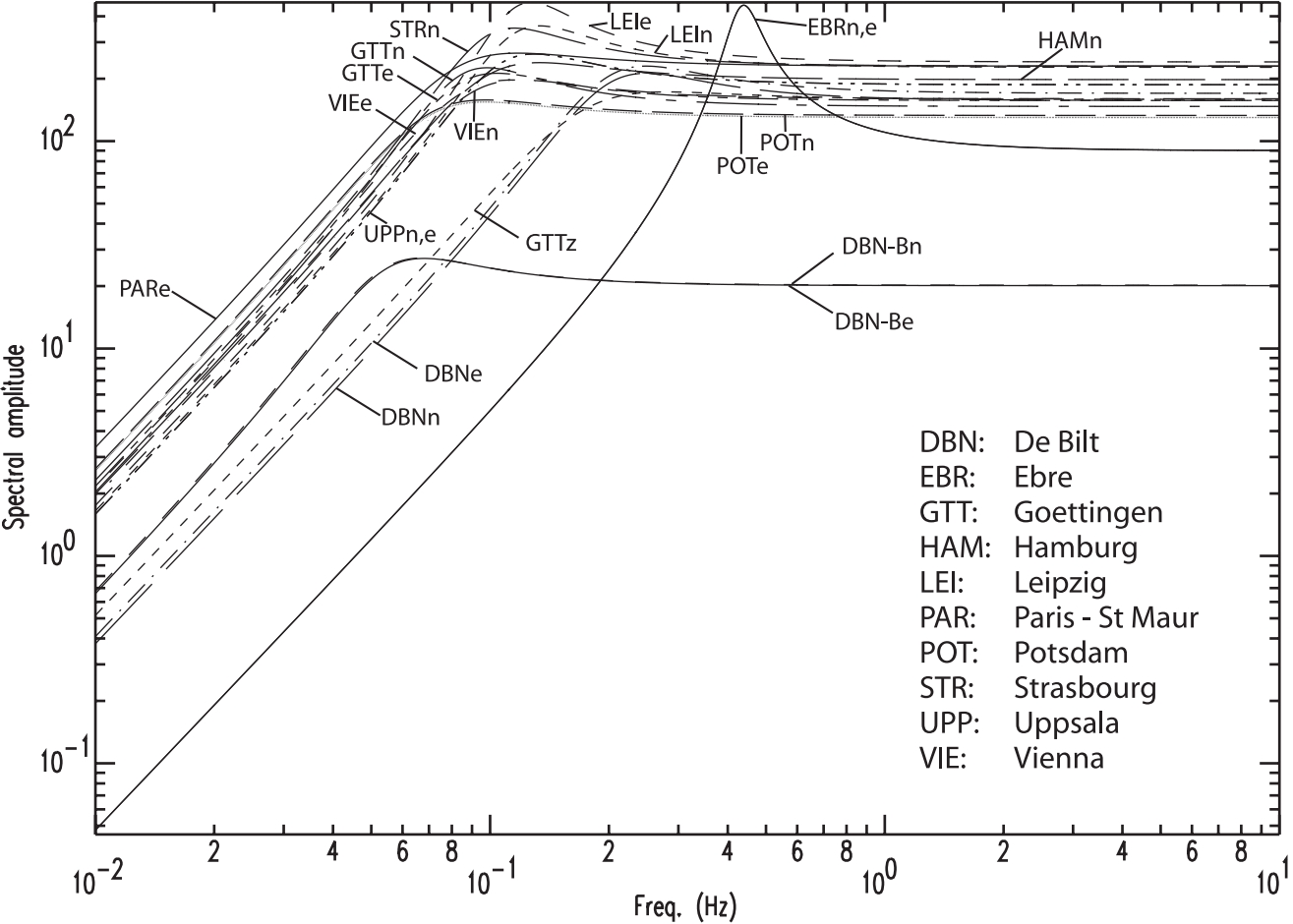
STRn
GTTn
GTTe
VIEe
VIEn
LEIe
LEIn
EBRn,e
HAMn
POTn
POTe
UPPn,e
GTTz
DBN-Bn
DBN-Be
PARe
DBNe
DBNn
DBN: De Bilt
EBR: Ebre
GTT: Goettingen
HAM: Hamburg
LEI: Leipzig
PAR: Paris - St Maur
POT: Potsdam
STR: Strasbourg
UPP: Uppsala
VIE: Vienna
Spectral amplitude
Freq. (Hz)

Figure 3

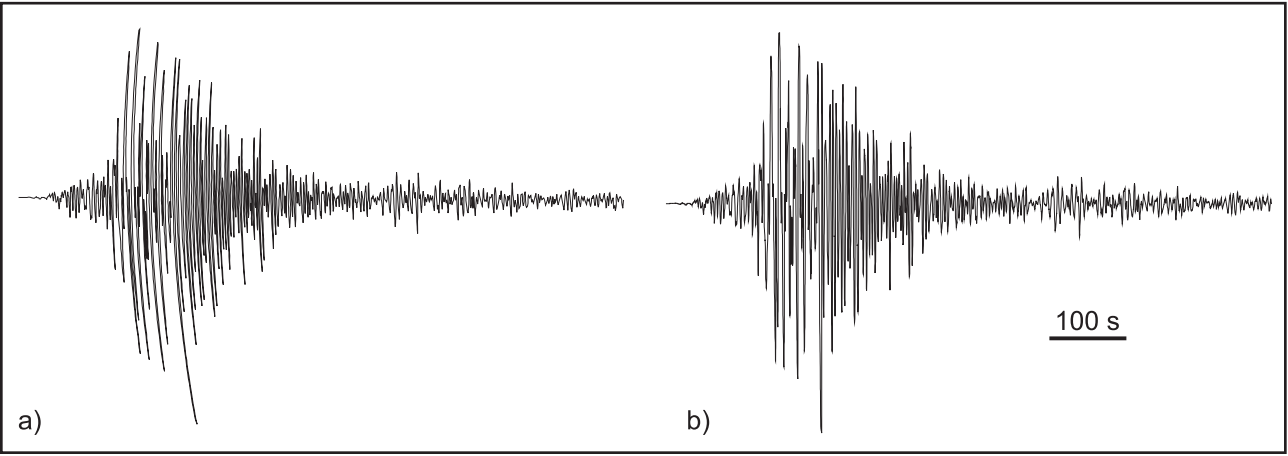

Figure 4

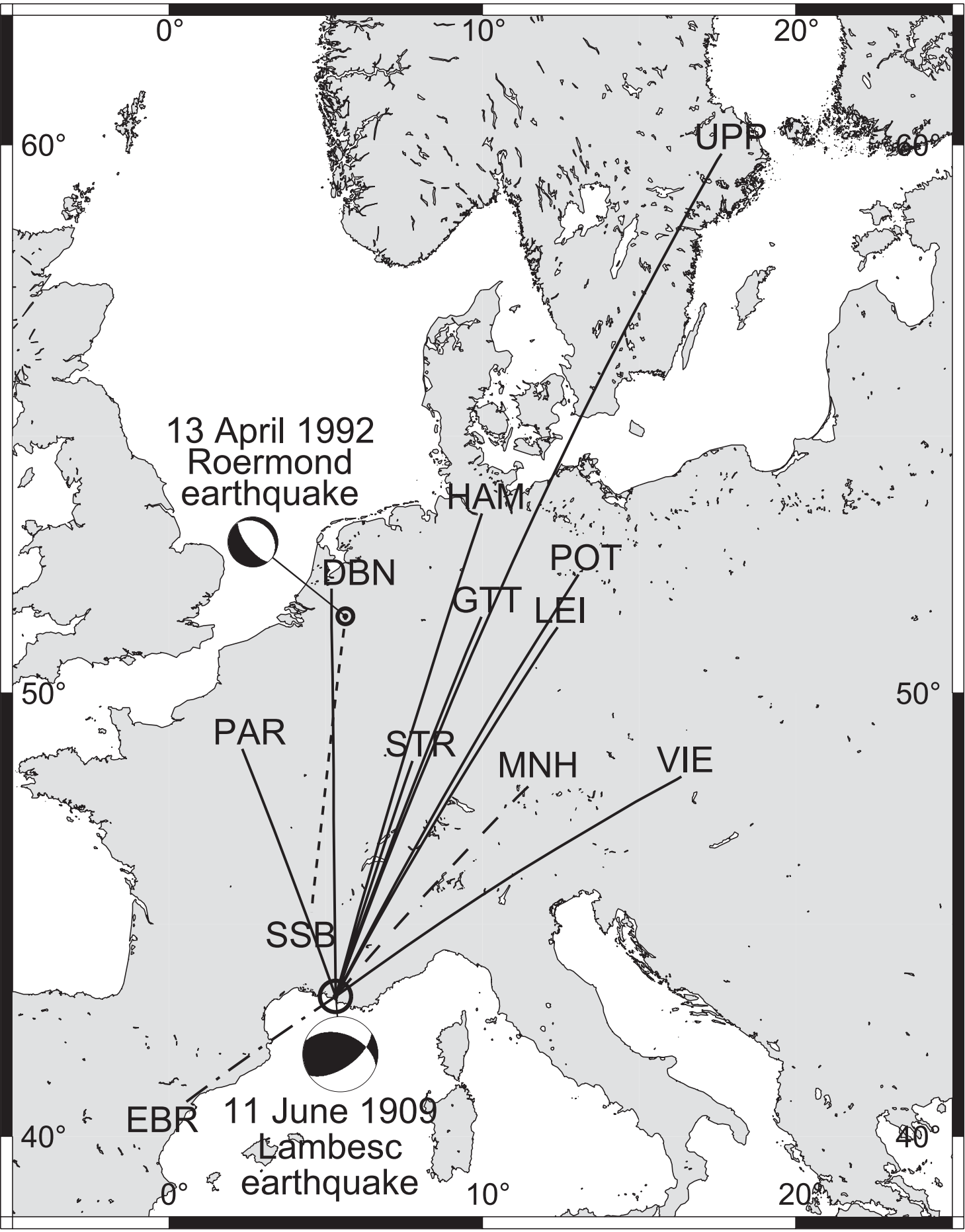
0°
10°
20°
60°
UPP
13 April 1992
Roermond
earthquake
HAM
POT
DBN
GTT
LEI
50°
PAR
STR
MNH
VIE
SSB
EBR
11 June 1909
Lambesc
earthquake
40°
0°
10°
20°

Figure 5

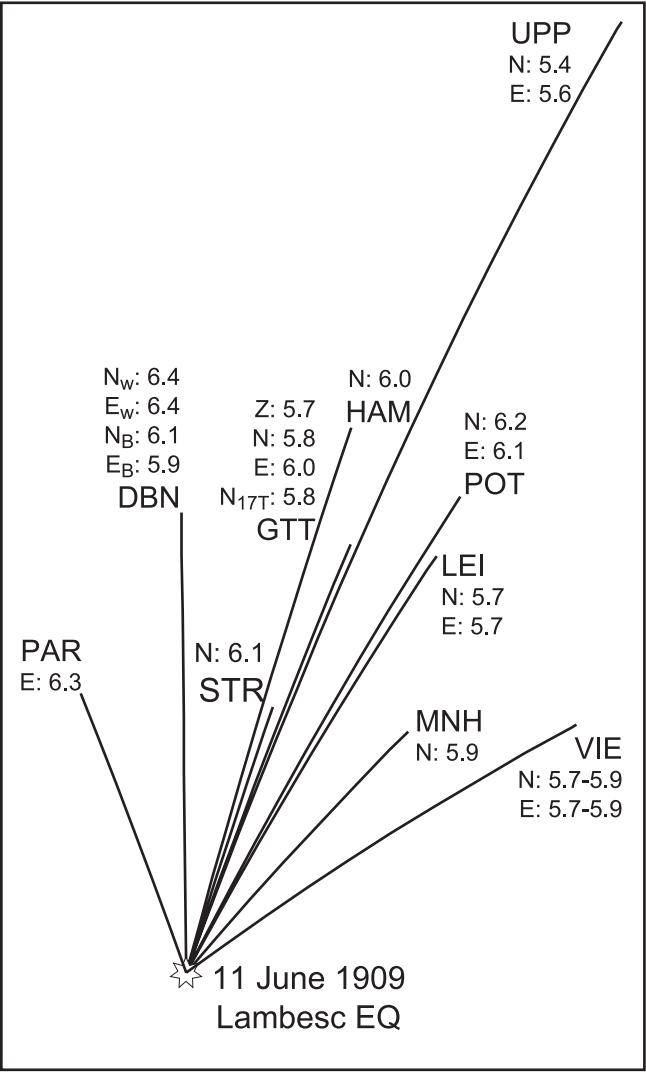
UPP
N: 5.4
E: 5.6
N: 6.0
HAM
Z: 5.7
N: 5.8
E: 6.0
N17T: 5.8
GTT
Nw: 6.4
Ew: 6.4
NB: 6.1
EB: 5.9
DBN
N: 6.2
E: 6.1
POT
LEI
N: 5.7
E: 5.7
PAR
E: 6.3
N: 6.1
STR
MNH
N: 5.9
VIE
N: 5.7-5.9
E: 5.7-5.9
11 June 1909
Lambesc EQ

Figure 6

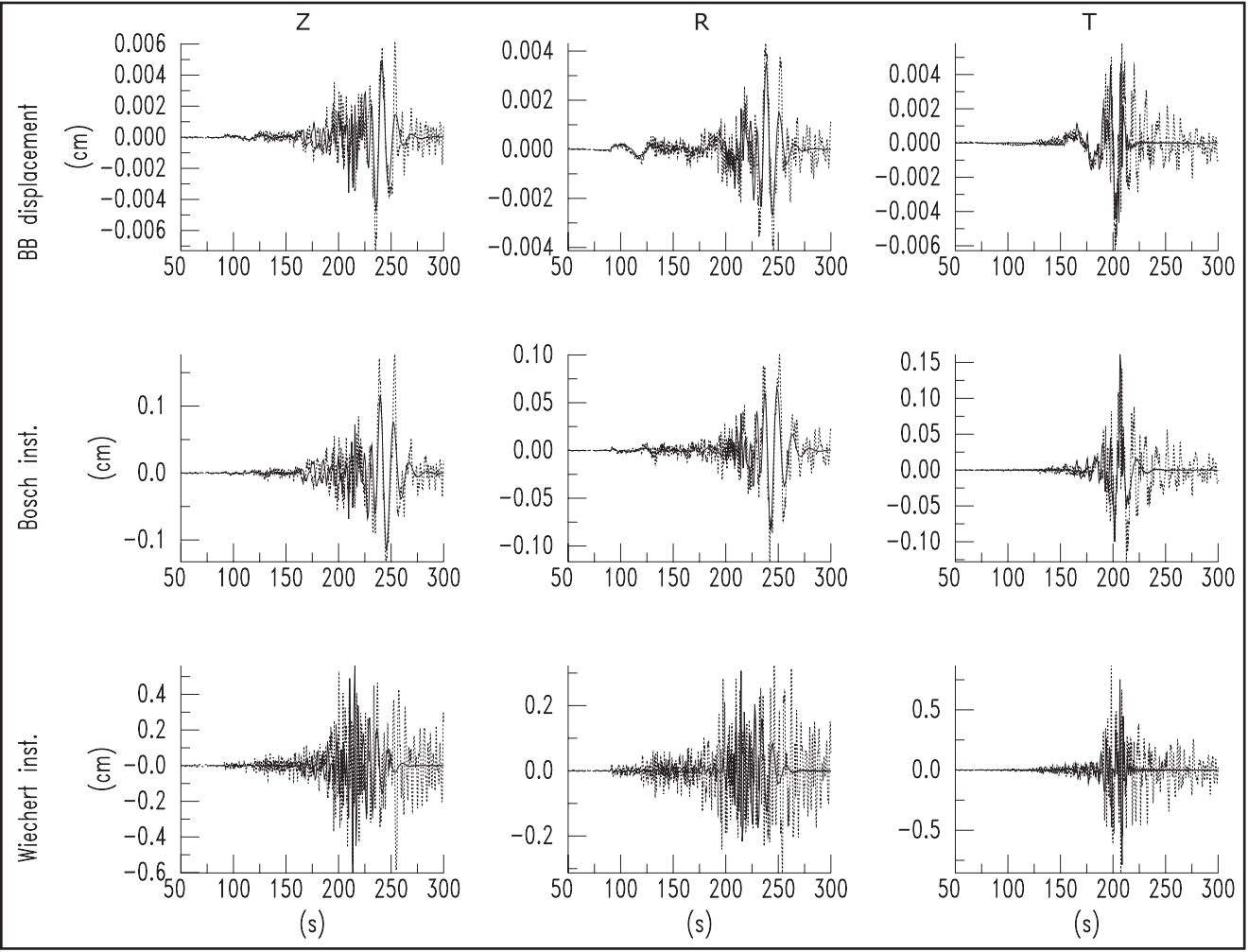
Z
R
T
BB displacement
Bosch inst.
Wiechert inst.
(cm)
(s)
0.006
0.004
0.002
0.000
−0.002
−0.004
−0.006
0.1
0.0
−0.1
0.10
0.05
0.00
−0.05
−0.10
0.15
0.4
0.2
−0.0
−0.2
−0.4
−0.6
0.5
−0.5
50
100
150
200
250
300

Figure 7

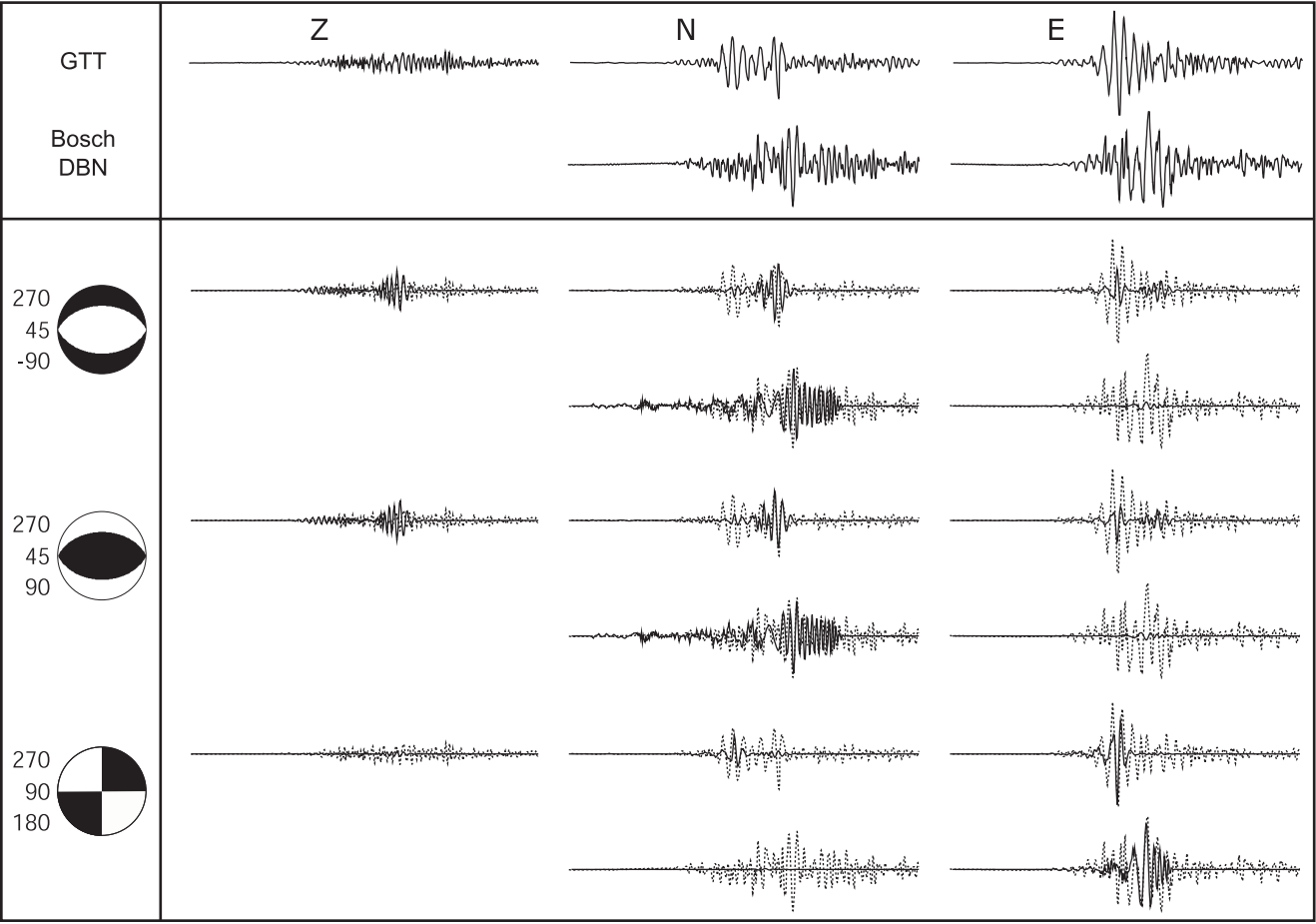

Figure 8

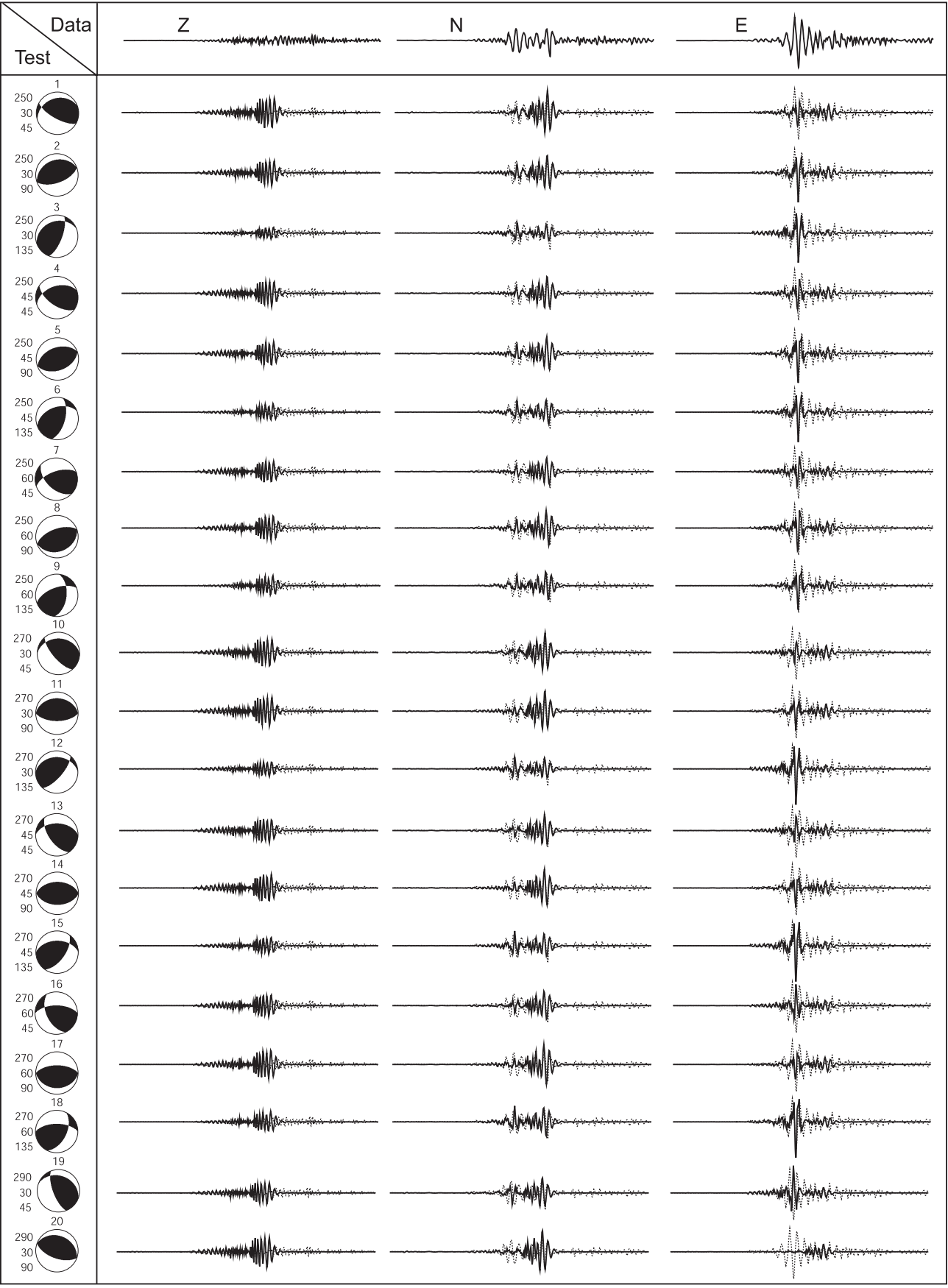
Data
Test
Z
N
E
1
250
30
45
2
250
30
90
3
250
30
135
4
250
45
45
5
250
45
90
6
250
45
135
7
250
60
45
8
250
60
90
9
250
60
135
10
270
30
45
11
270
30
90
12
270
30
135
13
270
45
45
14
270
45
90
15
270
45
135
16
270
60
45
17
270
60
90
18
270
60
135
19
290
30
45
20
290
30
90

Figure 9

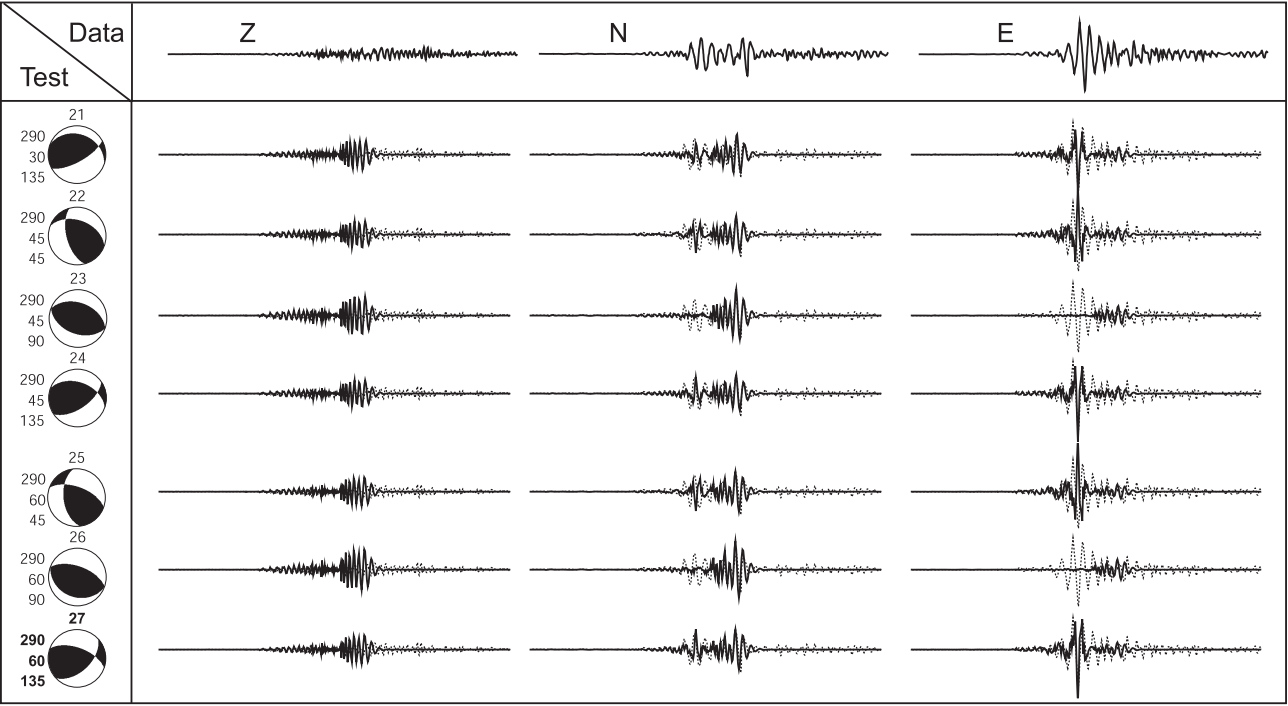

Figure 9 (continued)

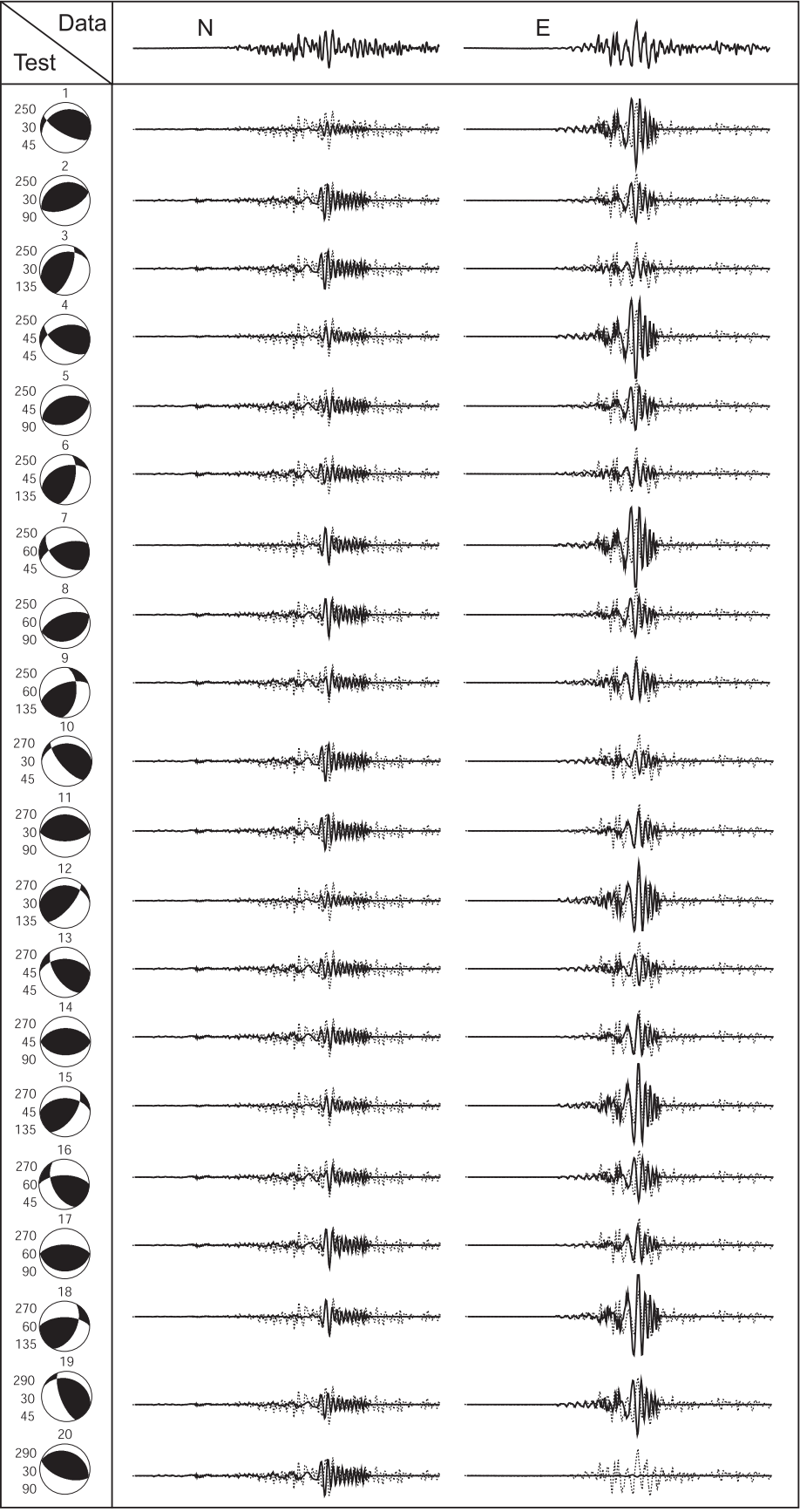
Data
Test
N
E
1
250
30
45
2
250
30
90
3
250
30
135
4
250
45
45
5
250
45
90
6
250
45
135
7
250
60
45
8
250
60
90
9
250
60
135
10
270
30
45
11
270
30
90
12
270
30
135
13
270
45
45
14
270
45
90
15
270
45
135
16
270
60
45
17
270
60
90
18
270
60
135
19
290
30
45
20
290
30
90

Figure 10

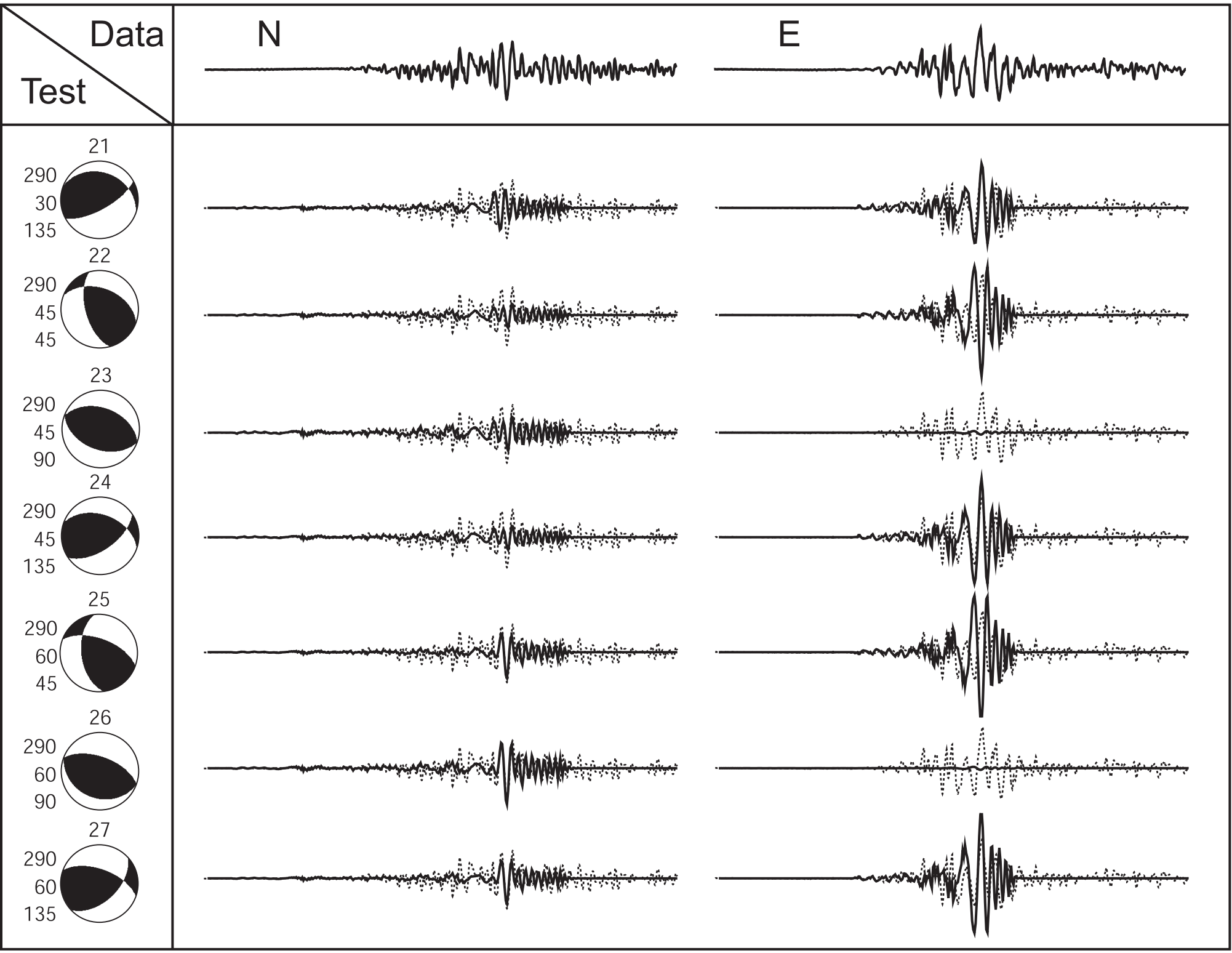

Figure 10 (continued)

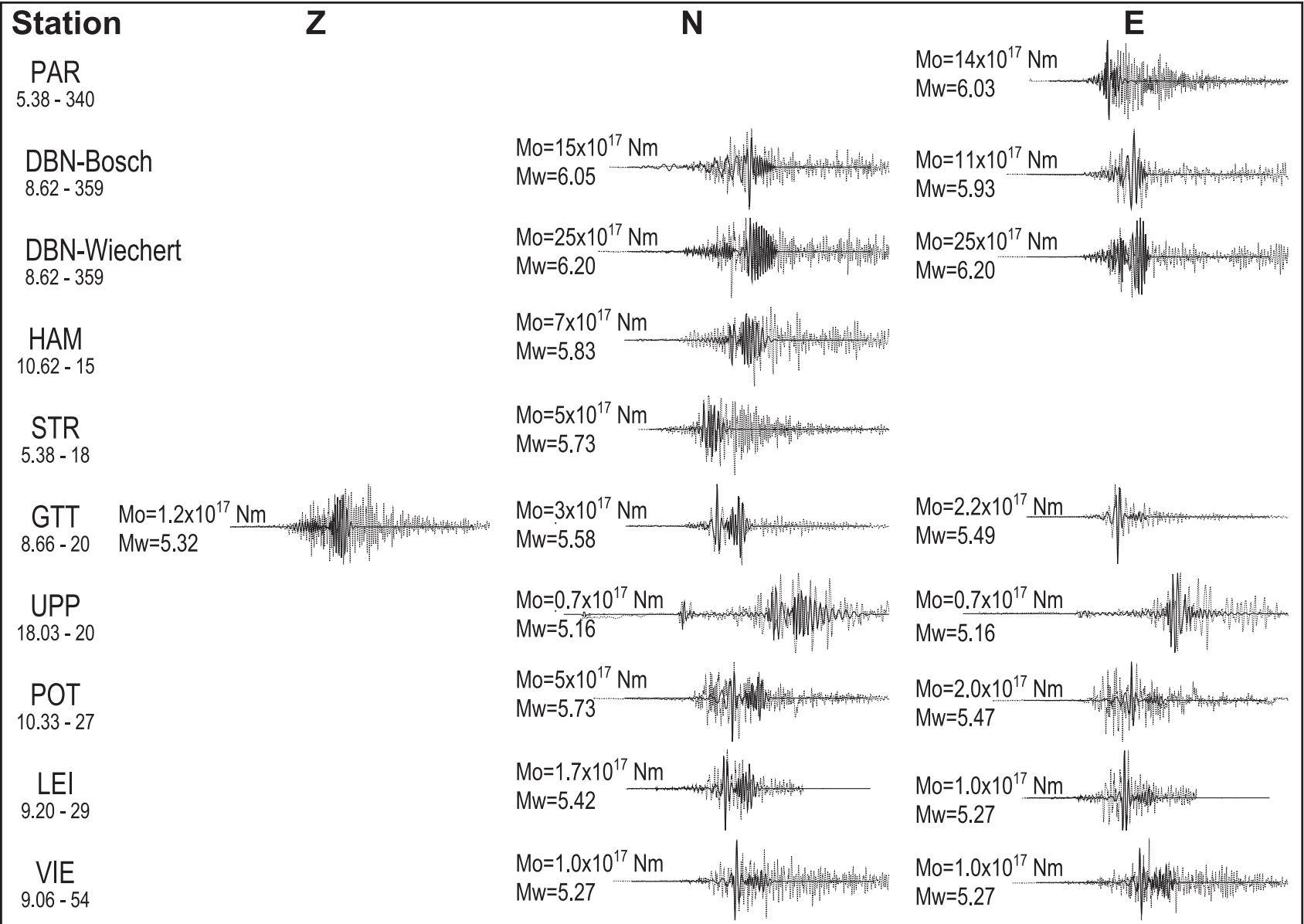
Station
Z
N
E
PAR
5.38 - 340
Mo=14x10^17 Nm
Mw=6.03
DBN-Bosch
8.62 - 359
Mo=15x10^17 Nm
Mw=6.05
Mo=11x10^17 Nm
Mw=5.93
DBN-Wiechert
8.62 - 359
Mo=25x10^17 Nm
Mw=6.20
Mo=25x10^17 Nm
Mw=6.20
HAM
10.62 - 15
Mo=7x10^17 Nm
Mw=5.83
STR
5.38 - 18
Mo=5x10^17 Nm
Mw=5.73
GTT
8.66 - 20
Mo=1.2x10^17 Nm
Mw=5.32
Mo=3x10^17 Nm
Mw=5.58
Mo=2.2x10^17 Nm
Mw=5.49
UPP
18.03 - 20
Mo=0.7x10^17 Nm
Mw=5.16
Mo=0.7x10^17 Nm
Mw=5.16
POT
10.33 - 27
Mo=5x10^17 Nm
Mw=5.73
Mo=2.0x10^17 Nm
Mw=5.47
LEI
9.20 - 29
Mo=1.7x10^17 Nm
Mw=5.42
Mo=1.0x10^17 Nm
Mw=5.27
VIE
9.06 - 54
Mo=1.0x10^17 Nm
Mw=5.27
Mo=1.0x10^17 Nm
Mw=5.27

Figure 11

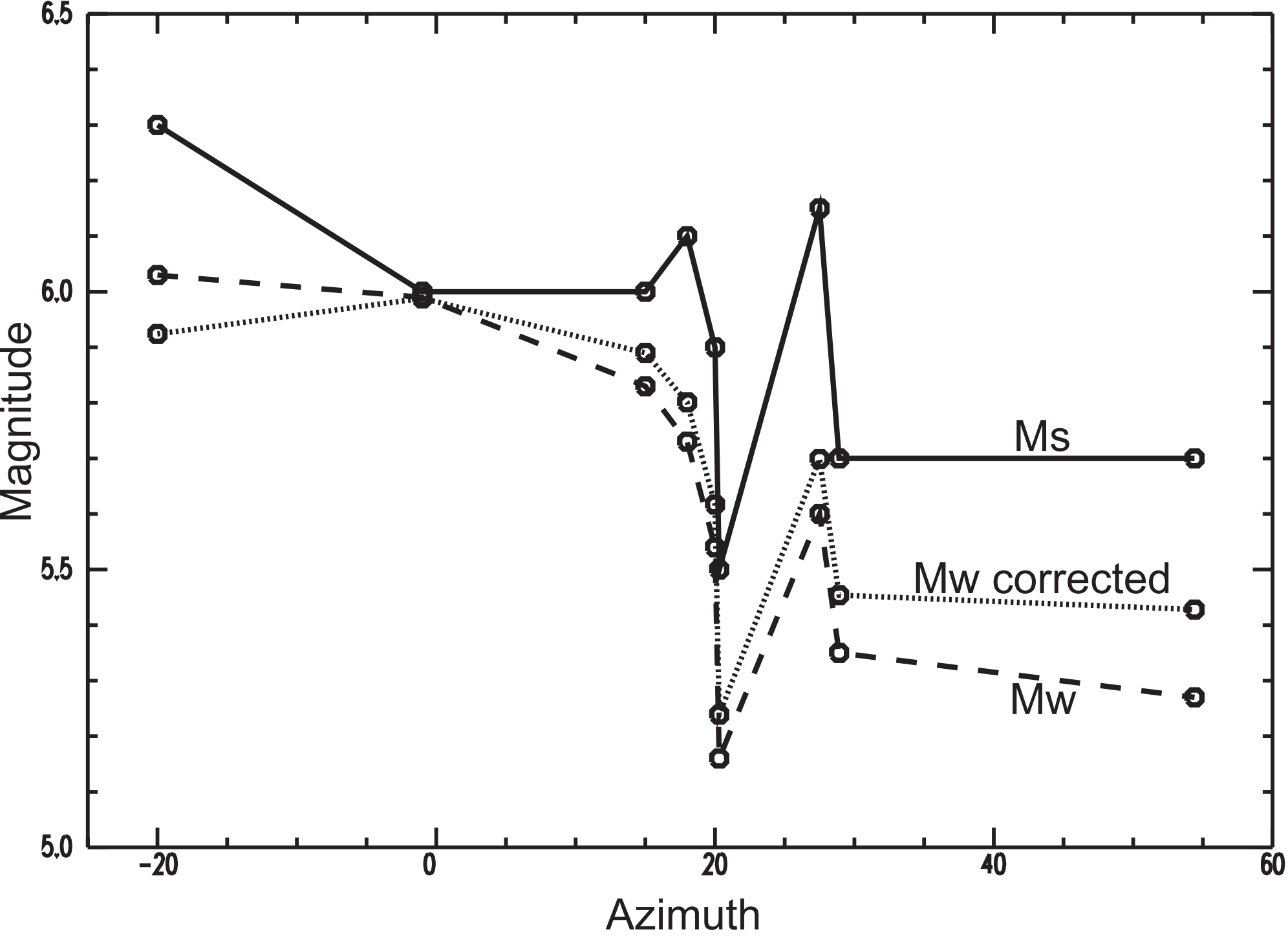

Figure 12

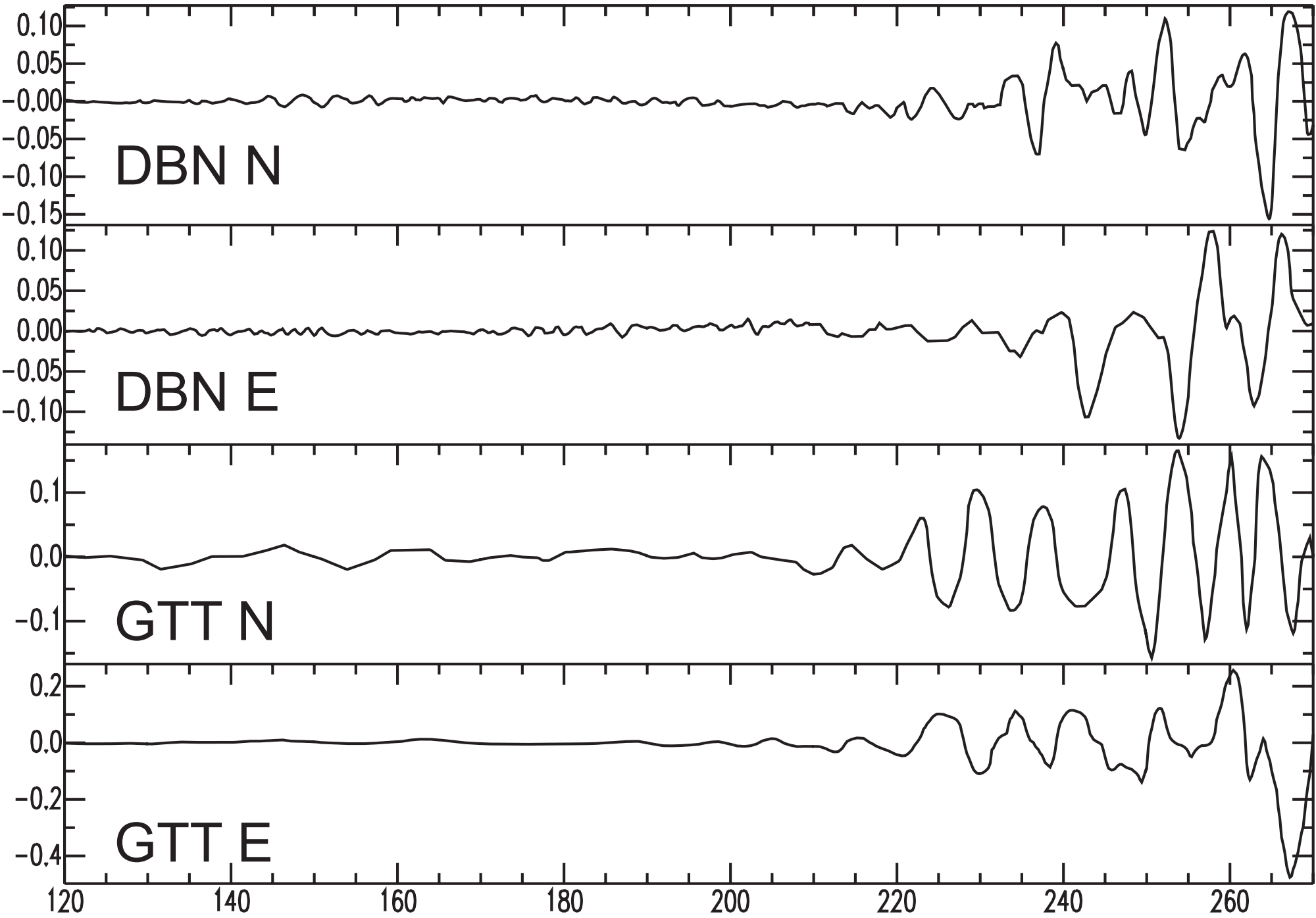
0.10
0.05
-0.00
-0.05
-0.10
-0.15
DBN N
0.10
0.05
0.00
-0.05
-0.10
DBN E
0.1
0.0
-0.1
GTT N
0.2
0.0
-0.2
-0.4
GTT E
120
140
160
180
200
220
240
260

Figure 13

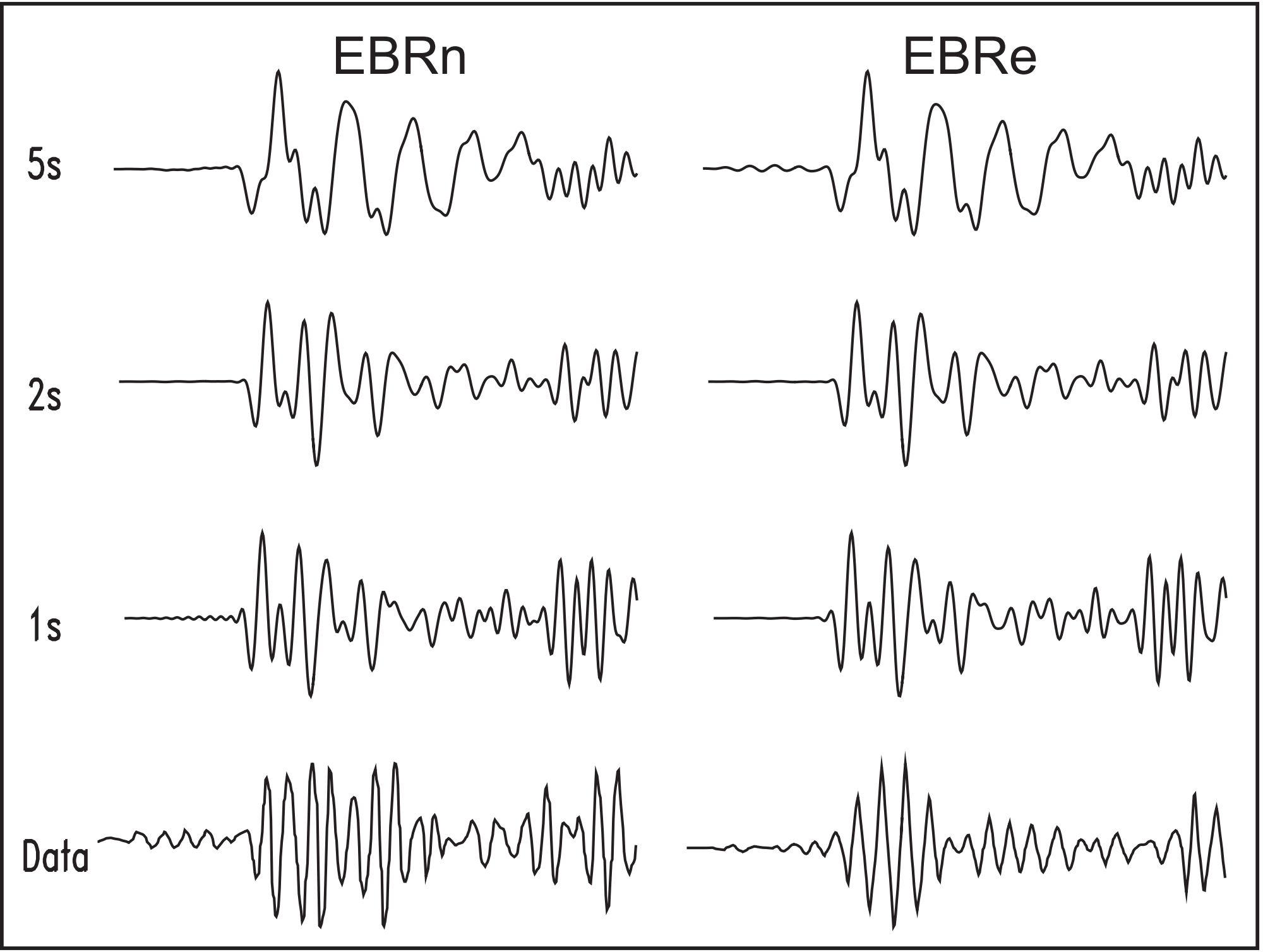

Figure 14

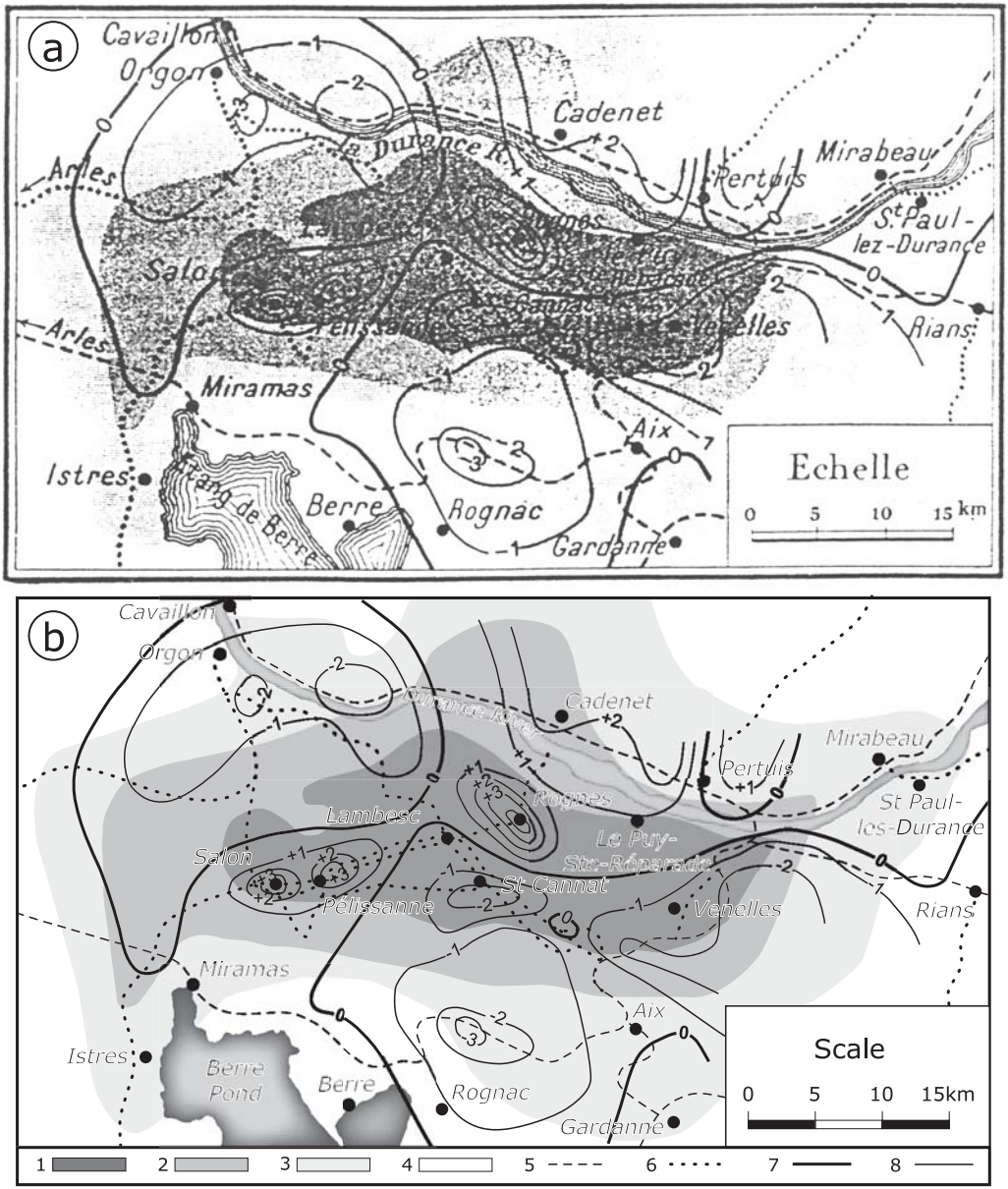
a
Cavaillon
Orgon
Arles
Cadenet
La Durance R.
Mirabeau
Pertuis
St Paul-
lez-Durance
Salon
Rians
Miramas
Aix
Istres
Etang de Berre
Berre
Rognac
Gardanne
Echelle
0 5 10 15 km
b
Cavaillon
Orgon
Durance River
Cadenet
Mirabeau
Pertuis
St Paul-
les-Durance
Lambesc
Rognes
Le Puy-
Ste-Réparade
Salon
St Cannat
Pélissanne
Venelles
Rians
Miramas
Aix
Istres
Berre
Pond
Berre
Rognac
Gardanne
Scale
0 5 10 15km
1 2 3 4 5 6 7 8

Figure 15

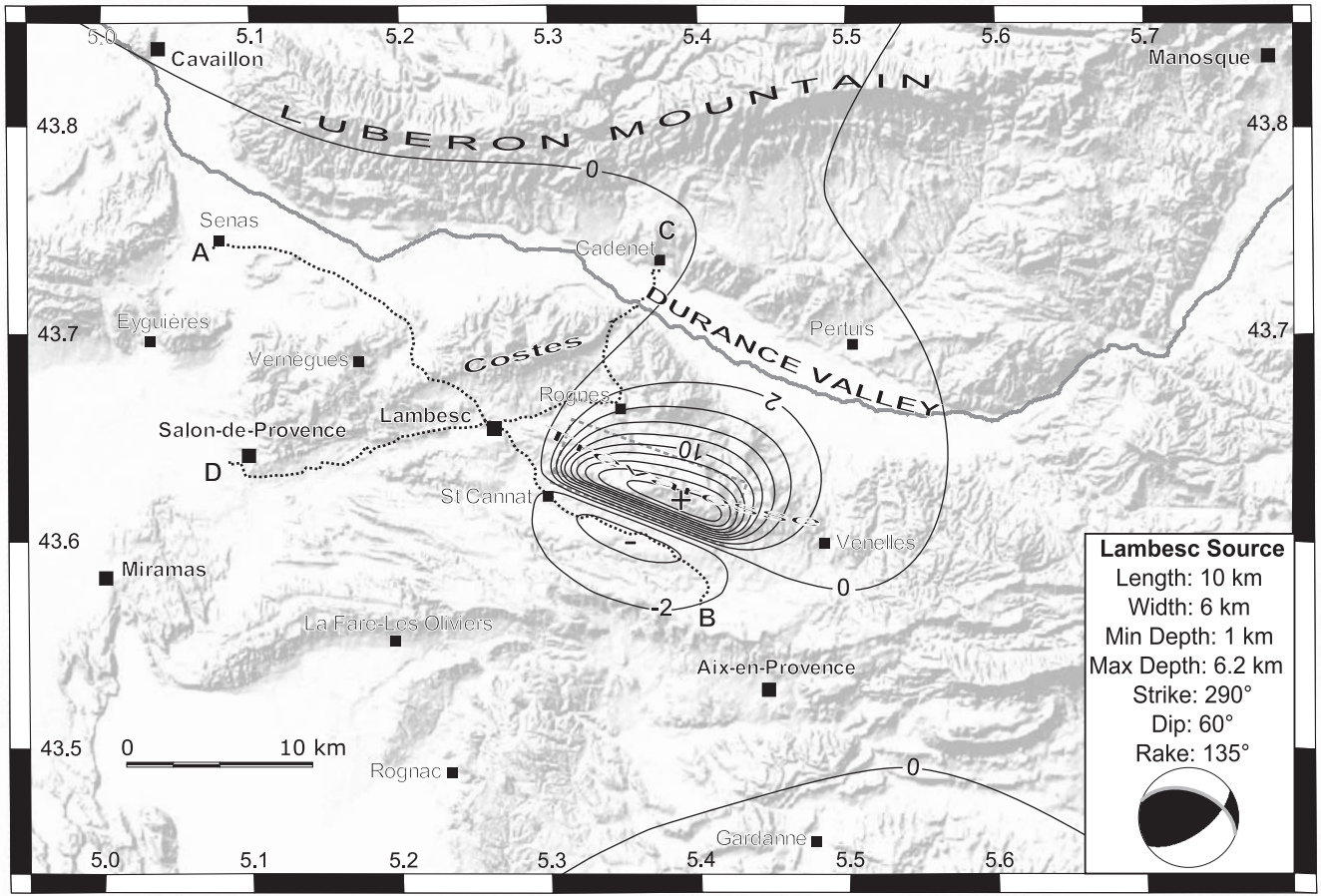
5.0
5.1
5.2
5.3
5.4
5.5
5.6
5.7
Cavaillon
Manosque
LUBERON MOUNTAIN
43.8
43.8
0
Senas
A
C
Cadenet
DURANCE VALLEY
Eyguières
43.7
Pertuis
43.7
Vernègues
Costes
Rognes
2
Salon-de-Provence
Lambesc
10
D
St Cannat
+
43.6
Venelles
Miramas
-
0
-2
B
La Fare-Les Oliviers
Aix-en-Provence
43.5
0
10 km
Rognac
0
Gardanne
5.0
5.1
5.2
5.3
5.4
5.5
5.6
Lambesc Source
Length: 10 km
Width: 6 km
Min Depth: 1 km
Max Depth: 6.2 km
Strike: 290°
Dip: 60°
Rake: 135°

Figure 16

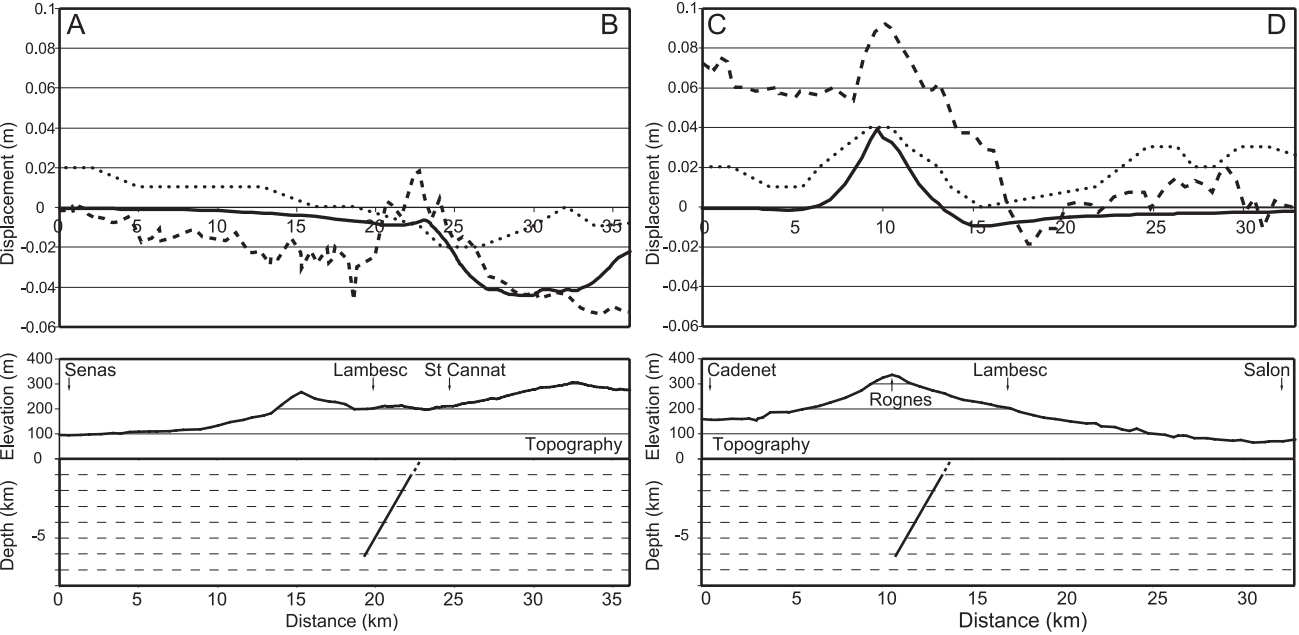
A
B
C
D
Displacement (m)
0.1
0.08
0.06
0.04
0.02
0
-0.02
-0.04
-0.06
0
5
10
15
20
25
30
35
Elevation (m)
400
300
200
100
0
Senas
Lambesc
St Cannat
Topography
Cadenet
Rognes
Salon
Depth (km)
-5
Distance (km)

Figure 17